frontiers in Physics

REVIEW
published: 18 January 2021
doi: 10.3389/fphy.2020.616618

Dual-Modal Photoacoustic Imaging and Optical Coherence Tomography [Review]

*Zohreh Hosseinaee, James A. Tummon Simmons and Parsin Haji Reza**

PhotoMedicine Labs, Department of System Design Engineering, University of Waterloo, Waterloo, Canada

Optical imaging technologies have enabled outstanding analysis of biomedical tissues through providing detailed functional and morphological contrast. Leveraging the valuable information provided by these modalities can help us build an understanding of tissues' characteristics. Among various optical imaging technologies, photoacoustic imaging (PAI) and optical coherence tomography (OCT) naturally complement each other in terms of contrast mechanism, penetration depth, and spatial resolution. The rich and unique molecular-specified absorption contrast offered by PAI would be well complemented by detailed scattering information of OCT. Together these two powerful imaging modalities can extract important characteristic of tissue such as depth-dependent scattering profile, volumetric structural information, chromophore concentration, flow velocity, polarization properties, and temperature distribution map. As a result, multimodal PAI-OCT imaging could impact a broad range of clinical and preclinical imaging applications including but not limited to oncology, neurology, dermatology, and ophthalmology. This review provides an overview of the technical specs of existing dual-modal PAI-OCT imaging systems, their applications, limitations, and future directions.

Keywords: photoacoustic imaging, optical coherence tomogaphy, dual-modal bioimaging, photoacoustic tomography, photoacoustic microscopy

OPEN ACCESS

Edited by:
Jun Xia,
University at Buffalo, United States

Reviewed by:
Changhui Li,
Peking University, China
Ye Zhan,
University at Buffalo, United States

****Correspondence:***
Parsin Haji Reza
phajireza@uwaterloo.ca

Specialty section:
This article was submitted to Medical Physics and Imaging, a section of the journal Frontiers in Physics

Received: *12 October 2020*
Accepted: *04 December 2020*
Published: *18 January 2021*

Citation:
Hosseinaee Z, Tummon Simmons JA and Reza PH (2021) Dual-Modal Photoacoustic Imaging and Optical Coherence Tomography [Review]. Front. Phys. 8:616618. doi: 10.3389/fphy.2020.616618

INTRODUCTION

The field of medical imaging has continued to grow quickly since the turn of the century, with many new modalities becoming a critical step in a variety of different disease care pathways. Novel imaging technologies continue to be developed, opening new routes to valuable functional and morphological information. Each imaging modality has its own specific strength and intrinsic limitations, such as spatial resolution, penetration depth, contrast mechanism, and sensitivity leading to precise and reliable images correlated with true anatomy. To compensate the weak aspects of different modalities, multimodal imaging concepts have been considered in recent years [1–3]. Multimodal imaging can play an important role in the clinical care of various diseases by improving the clinician's ability to perform monitoring, surveillance, staging, diagnosis, planning and therapy guidance, screening therapy efficacy, and evaluating recurrence [2]. Multimodal imaging systems have been widely used in medical research and clinical practice, such as cardiovascular diseases [4, 5], neuropsychiatric diseases [6], Alzheimer [7], and tumor resection surgeries [8].

Photoacoustic imaging (PAI) is one recent example of the successful rise of a novel optical imaging modality. PAI uses the absorption characteristics of specific endogenous or exogenous biomarkers to generate targeted image contrast with a wide scalable range of spatial resolution and penetration depths [9, 10]. The rich absorption information that PAI provides would be well

complemented by an imaging modality which offers detailed scattering information. Optical coherence tomography (OCT) is a well-established imaging technology which can provide excellent depth-resolved morphological information. OCT is currently used in a broad range of clinical applications and is a standard of care in the field of ophthalmology for the diagnosis of various critical eye diseases [11–13]. OCT is considered as an ideal companion for PAI by providing complementary imaging contrast, strongly motivating the development of multimodal PAI and OCT systems. While OCT can image microanatomy of biological tissues, PAI devices could provide detailed molecular and metabolic information of the sample [14–16]. This multimodal system could provide access to valuable information about biological tissues and has the potential to impact a broad range of clinical and preclinical imaging applications including but not limited to oncology, neurology, dermatology, and ophthalmology. In this review, we first introduce the basic mechanisms of PAI and OCT and discuss their current applications. Then, we compare PAI and OCT, contrasting the strengths and limitations of each modality while highlighting the potential applications of a multimodal system. Finally, we review the development of existing dual-modal systems, emphasizing their strengths along with the challenges they need to overcome to move to the clinic.

PHOTOACOUSTIC IMAGING: PRINCIPLES AND APPLICATIONS

Photoacoustic imaging is among the most rapidly growing technologies in biomedical imaging [17, 18]. The modality is based on the photoacoustic effect, which was discovered by Bell in 1880 [19]. In general, once the tissue is irradiated by short laser pulses, endogenous or exogenous chromophores inside the tissue absorb the photon's energy. This absorbed energy then induces a transient local temperature rise, which in turn generates pressure waves through thermoelastic expansion. These pressure waves, which propagate in tissue as ultrasound signals, can be captured by acoustic detectors to form images of the chromophore's distribution inside the sample [20]. Depending on the spatial scales of optical absorbers, the frequency content of generated ultrasound signals might extend to several tens or even hundreds of megahertz. The bandwidth of this signal and corresponding spatial resolution is not limited by the PA generation process. Instead, the frequency-dependent acoustic attenuation happening in soft tissue limits the maximum frequency content of PA wave and therefore defines the achievable spatial resolution. As a result, the spatial resolution in PAI scales with depth. In addition, ultrasound detector's properties such as bandwidth, center frequency, element size, and detection aperture can limit the spatial resolutions of PAI devices [21].

Based on the way images are formed, PAI can be split into two main categories: photoacoustic tomography (PAT), which uses reconstruction-based image formation, and photoacoustic microscopy (PAM) which uses focused-based image formation [22]. In photoacoustic tomography, usually a widefield unfocused excitation beam is used together with an array of ultrasonic detectors which measure the generated ultrasound waves in multiple positions simultaneously [23–25]. It can provide large field of view (FOV) images and has been used in applications such as whole-body imaging of small animals [26] and breast cancer studies [27]. In contrast to PAT, PAM is based on raster-scanning of optical and acoustic foci and forms images directly from recorded depth-resolved signals [28]. Generally, PAM is the preferred configuration for use in applications which require high resolution over deep penetration depth, for example, in single-cell imaging [29]. PAM can be further divided into acoustic-resolution PAM (AR-PAM), where the acoustic focusing is tighter than optical focusing [30], and optical-resolution PAM (OR-PAM), where the optical focusing dominates the resolution [31]. **Figure 1** demonstrates the imaging setup for different possible configurations of photoacoustic imaging systems. Photoacoustic endoscopy (PAE) can be considered as a subcategory of both PAM and PAT (depending on the implementation), which is applied for imaging internal tissue/organs and usually provides micron-scale spatial resolution and millimeter-scale imaging depth [32].

Photoacoustic imaging devices offer two distinct advantages which primarily stem from the combination of optical excitation and acoustic detection. First, they provide the unique imaging contrast of optical absorption. As a result, PAI enables high-sensitivity detection of endogenous chromophores which are weakly fluorescent and difficult or impractical to be labeled with exogenous fluorophores, including but not limited to hemoglobin, melanin, collagen, cytochrome, and lipid [33]. This complements established imaging technologies including fluorescence imaging, which is currently one of the leading technologies for *in vivo* optical molecular imaging [34]. Second, PAI enables a wide scalable range of spatial resolution and penetration depths across macroscopic (i.e., 100-400 μm resolution at the depth of several centimeters) [18], mesoscopic (i.e., tens of micrometer resolution at the depth of 1–10 mm) [35], and microscopic (i.e., micrometer resolution at the depth of submillimeter) [36]. Additionally, the modality has practical functional and molecular imaging capabilities making it a powerful tool for biomedical investigations [21]. One of these well-known capabilities is photoacoustic spectroscopy which is based on the ability to selectively image specific chromophores by tuning the excitation wavelength [37]. Here, by acquiring images at multiple wavelengths and undertaking spectroscopic analysis, the concentration of specific chromophores can be quantified. For example, in the visible and NIR wavelength, the absorption spectrum of blood is highly dependent on its oxygen saturation (SO_2) and consequently the significant spectral difference between oxyhemoglobin (HbO_2) and deoxyhemoglobin (HHb). Using this spectral difference, it is possible to quantify the concentration of HbO_2 and HHb and estimate SO_2 which is an important physiological parameter related to several pathophysiological processes and inflammatory conditions. Other functional extensions of PAI such as Doppler flowmetry [38, 39] and photoacoustic thermometry [40, 41] have enabled measurement of blood flow velocity and acquiring maps of temperature distributions in tissue, respectively.

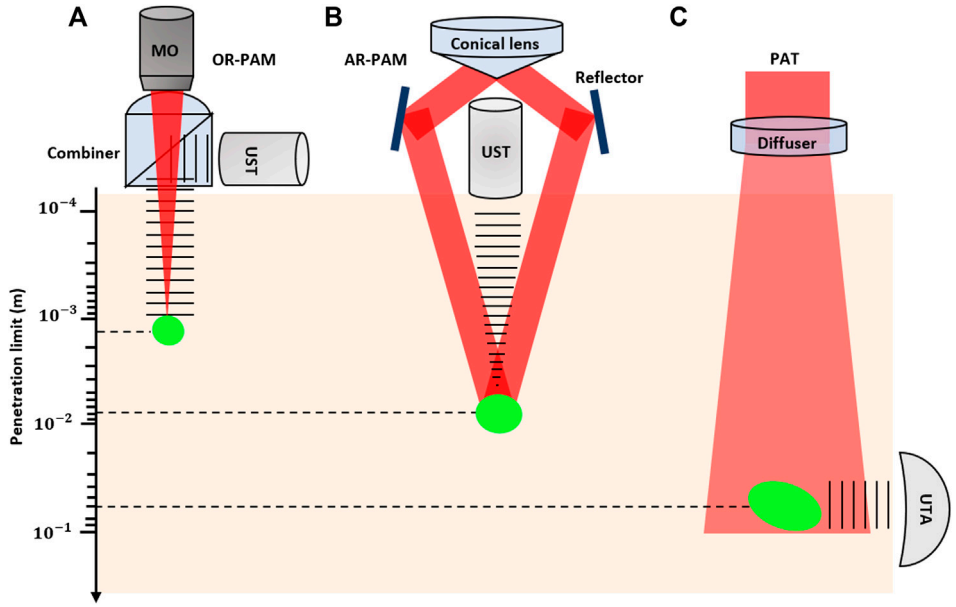

FIGURE 1 | Signal generation and detection in different implementations of PAI and penetration limits in scattering tissue. **(A)** Reflection-mode OR-PAM system with an optical–acoustic combiner that transmits light but reflects sound; **(B)** AR-PAM system where the laser light is poorly focused; **(C)** PAT system with ultrasonic transducer array (UTA). The laser beam is expanded and homogenized by a diffuser to provide widefield illumination.

These unique and important imaging advantages offered by PAI make it the preferred modality for a broad range of functional and molecular imaging applications. It has been used in numerous preclinical and clinical applications including but not limited to blood oxygen saturation imaging [42, 43], brain vasculature and functional imaging [44, 45], gene expression [46], vulnerable atherosclerotic plaques diagnosis [47], skin melanomas [48], histology-like tissue imaging [49, 50], longitudinal tumor angiogenesis studies [51], imaging and detection of protein interactions [52], ophthalmic imaging [53], and tissue engineering scaffolds [54].

OPTICAL COHERENCE TOMOGRAPHY: PRINCIPLES AND APPLICATIONS

Optical coherence tomography (OCT) is an optical imaging technique with high-resolution structural content. Unlike photoacoustic imaging, OCT obtains its imaging contrast from optical scattering of internal tissue microstructures and can be considered as an optical analogy to ultrasound pulse echo imaging [55]. The modality is based on the principles of low-coherence interferometry, where a low-coherence light beam is directed on to the targeted tissue. The backscattered light is combined with a reference beam, which was split off from the original light beam. The resulting interference patterns are used to reconstruct cross-sectional images, which represent the reflectivity profile of the tissue along the beam path [56, 57].

The first generation of OCT known as time domain OCT (TD-OCT) was developed in the 1990s [55]. The technology required acquisition of a depth scan for every location and subsequently suffered from slow imaging speed and poor image quality that limited adoption of the technology. The introduction of Fourier domain OCT (FD-OCT) overcame these limitations by providing a more efficient implementation of low-coherence interferometry principles [58]. Unlike TD-OCT, FD-OCT uses spectral information to generate a depth profile without the need for mechanical scanning of the optical path length [59]. It offers >100x improvement of the image acquisition rate and >20 dB signal-to-noise ratio (SNR) compared to TD-OCT systems.

Depending on whether spectral information in FD-OCT is separated at the system's input (tunable laser) or system's detection end (spectrometer), FD-OCT systems can be classified into two major groups: spectral-domain OCT (SD-OCT) in which a broad bandwidth light source is used as the interferometer input and a spectrometer with a linear array camera at the interferometer output, or swept-source OCT (SS-OCT), which uses a tunable laser as the interferometer input and a single photodiode at the interferometer output [60]. **Figure 2** depicts schematic of different OCT modalities.

OCT technology has enabled noncontact, high speed, cross-sectional imaging over a large field of view with submicron resolution in biological tissues. It is currently the preferred technology in ophthalmology for corneal imaging, as well as retinal structural and vascular imaging [61–63]. Various functional extensions of OCT have been developed including: Doppler OCT [64], OCT angiography (OCTA) [65], polarization sensitive OCT (PS-OCT) [66], OCT elastography [67], and

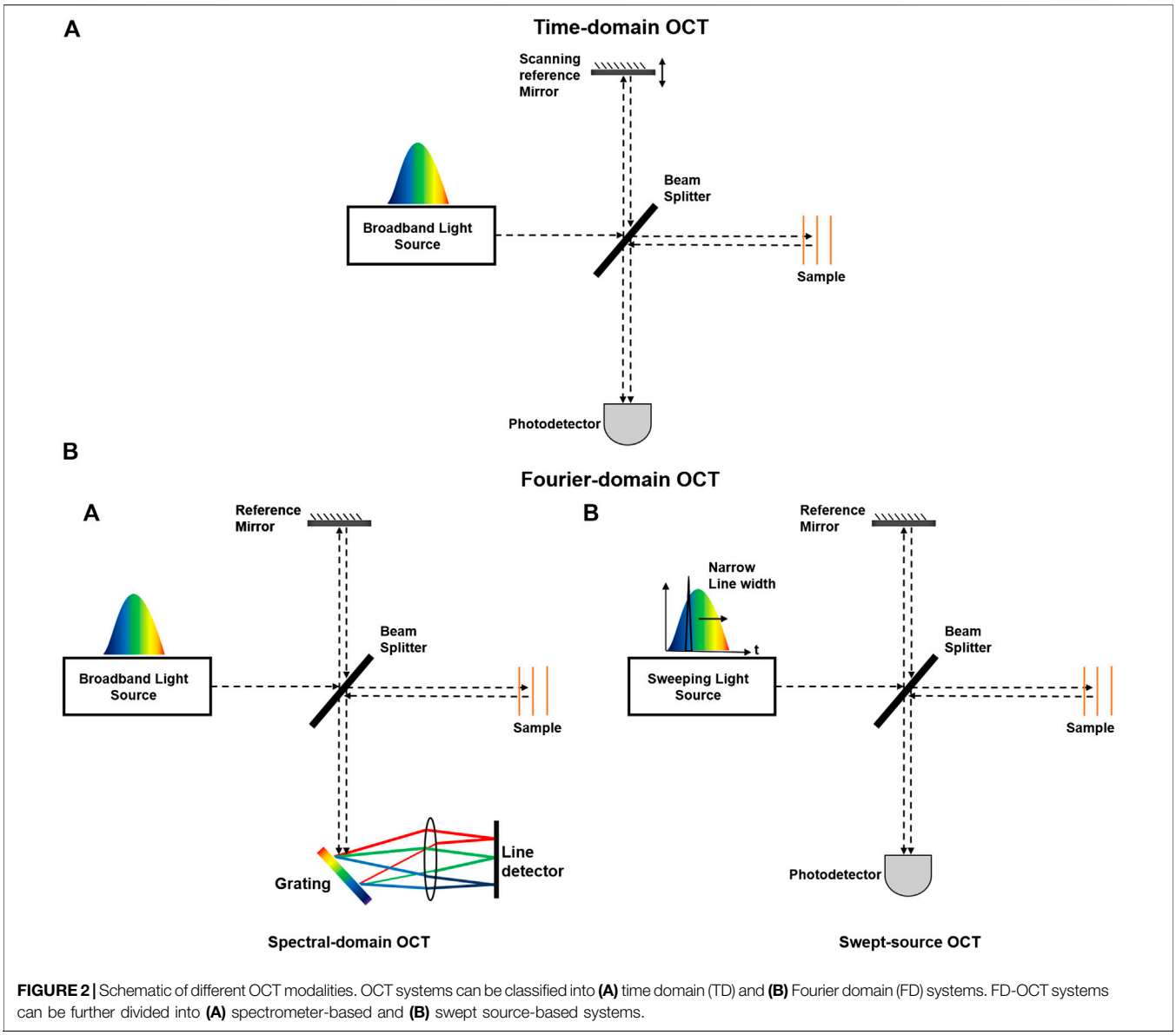

FIGURE 2 | Schematic of different OCT modalities. OCT systems can be classified into **(A)** time domain (TD) and **(B)** Fourier domain (FD) systems. FD-OCT systems can be further divided into **(A)** spectrometer-based and **(B)** swept source-based systems.

spectroscopic OCT [68]. Besides ophthalmic applications, OCT has been applied in other clinical applications such as brain imaging [69, 70], tissue engineering [71], cardiology and cardiovascular imaging [72], skin imaging [73], neuroimaging [74], gynecology [75], oncology [76], and dental imaging [77].

Due to highly scattering nature of biological tissues and the contrast mechanism of OCT, the penetration depth of OCT devices is limited to be within a few millimeters [13]. In addition, OCT relies on variation in scattering information to derive useful imaging contrast about the sample, making it unable to effectively image interconnected soft tissues with similar scattering properties. To provide additional contrast information, efforts have been made to integrate OCT with other optical imaging modalities such as multiphoton microscopy [78] and confocal microscopy [79]. While these technologies provide new contrast information, they both rely on fluorescence as their contrast mechanism. In addition, they cannot enhance the depth information that OCT devices currently obtain.

DUAL-MODAL PHOTOACOUSTIC IMAGING AND OPTICAL COHERENCE TOMOGRAPHY

The performance characteristics of PAI and OCT imaging systems make them a suitable companion for a multimodal imaging system. A brief comparison of important features of both PAI and OCT modalities is given in **Table 1**. The spatial resolution of both modalities is highly dependent on their implementation and can range from submicron resolution for OCT [80, 81] and OR-PAM [36] to a few hundreds of micron in

TABLE 1 | Comparison of photoacoustic imaging and optical coherence tomography.

Imaging parameter	Photoacoustic imaging	Optical coherence tomography
Axial resolution	Determined by the detected photoacoustic bandwidth, usually several tens of microns	Determined by the central wavelength and coherence length of the light source, generally within a few microns
Lateral resolution	Depending on the implementation can range from ~0.3 to 400 μm	Determined by the central wavelength of the light source and imaging optics, usually within tens of microns
Imaging depth	Depending on the implementation range from ~1.5 to ~ 7 cm	Restricted by the optical transport mean free path ~2 mm
Imaging speed	Defined by the laser pulse repetition rate, mechanical scanning speed, or the multiplexed data acquisition time	Usually defined by the sweep rate of laser or speed of spectrometer's camera
Contrast mechanism	Absorption	Scattering

PAT systems [82]. While available imaging depth of OCT is restricted by the optical transport mean free path to ~2 mm, AR-PAM and PAT systems can achieve imaging depth of a few millimeters [35] to a few centimeters [27], respectively. In terms of speed, both modalities offer a wide range of imaging speed with submilliseconds to a hundred of seconds range [83, 84], which should be chosen based on intended applications.

The complementary information of PAI and OCT makes them the favored modality for a wide range of imaging applications. For example, in blood flow imaging, OCT angiography and Doppler OCT could obtain high-resolution images based on the backscattering properties of moving red blood cells, while PAI would remain sensitive to all blood cells, regardless of their flowing state. Therefore, the integrated system provides a powerful tool for blood flow imaging in vascular diseases such as stroke, hemorrhage, vascular occlusions, or certain pathologies with flow stasis such as tumors [85, 86].

For spectroscopic analysis and blood oxygen saturation measurements, despite recent advances in the spectroscopic OCT [87–89], the technology is not background free and suffers from sensitivity to speckle noise and polarization changes. In addition, the scattering loses alter the spectral signal components and makes it difficult to quantify blood oxygen. On the other hand, spectroscopic PAI methods are well-established for quantifying blood oxygen saturation. This information would be well complemented with Doppler OCT flow measurements and help to quantify metabolic rate of oxygen consumption. This will open up a broad range of applications for pathophysiological conditions such as angiogenesis, tissue inflammatory, and healing responses. For example, in ophthalmology measuring, metabolic rate of oxygen is a sensitive biomarker for early-stage diagnosis and an indicator for progression of several retinal diseases including glaucoma, diabetic retinopathy, and age-related macular degeneration [90–93]. Alternatively, in oncology and metastasis detection, the spectroscopic and metabolic information available through the dual-modal PAI-OCT system could reveal changes in endogenous chromophore concentrations and be employed for differentiating normal and pathological tissues [94]. It may facilitate longitudinal assessment of tumor growth and evaluate treatment success of novel therapeutic agents [95, 96]. In brain imaging applications, this metabolic information can be used to extract brain oxygenation and metabolism of oxygen and glucose [97] and resting-state connectivity [98] and to study how the brain responds to various physiological and pathological conditions [99]. Furthermore, the fine vascular structure and subcellular features available through high spatial resolution of OCT and OR-PAM could facilitate diagnosis of brain disorders such as stroke, epilepsy, and edema [100–102].

The combination of PAI and OCT is a powerful tool in dermatology by providing detailed morphology and complete description map of skin perfusion. It enables studying the texture of skin and determines the margin of morphological changes caused by skin disorders [103]. The technique may overcome the limitations of histology-based margin assessment methodologies and facilitate tumor resections in surgical rooms [104, 105]. Subsequently, it can be used to improve the rate of complete excision and to reduce the average number of stages during Mohs micrographic surgery [106, 107]. The dual-modal imaging platform can be applied for studying a wide range of skin conditions such as melanoma tumors, vascular lesions, soft tissue damages such as wounds and burns, inflammatory conditions, and other superficial tissue abnormalities characterized by morphology and function of supplying vasculature [108].

The dual-modal PAI-OCT system could have a significant impact for endoscopic applications as well. Currently, most of endoscopic imaging devices rely on widefield white-light optical methods, which are limited by what the human eye can see and therefore suffer from lack of sensitivity to subsurface and physiological changes. The combination of deep tissue penetration and high resolution along with functional and molecular information makes PAI-OCT the favorable endoscope to observe inside the body and visualize physiological processes and microscopic features of tissues [109, 110]. The targeted molecular imaging may allow for the detection of small and invisible lesions in epithelial surfaces that line the internal organs such as gastrointestinal, pulmonary, and ductal. This information can be used to facilitate detecting cancer at early stages [111]. Another important application for endoscopic PAI-OCT would be intravascular atherosclerotic imaging, where the PAI subsystem could penetrate deep and provide molecular information about the plaque composition and OCT maintains high-resolution, depth-resolved scattering contrast for lipid rich plaques [112].

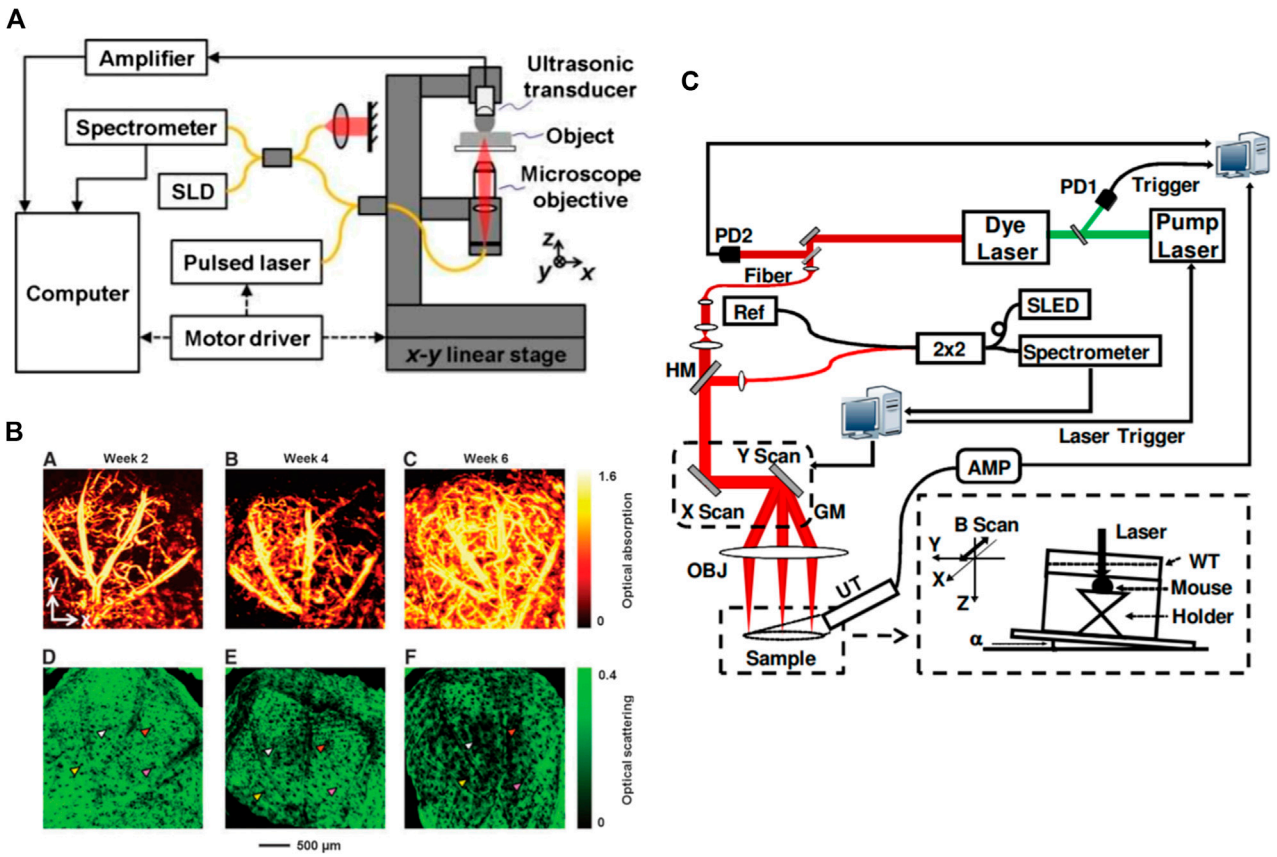

FIGURE 3 | (A) Schematic of the combined PAM-OCT. SLD: superluminescent diode. Solid lines represent single-mode optical fibers. Reprinted with permission from [113]; **(B)** PAM and OCT images showing the vasculature and tissue structure for an inverse scaffold with a pore size of 200 μm; **(A–C)** PAM images showing the development of blood vessels at 2, 4, and 6 weeks after implantation, respectively; **(D–F)** the corresponding OCT images showing the tissue structure. Reprinted with permission from [114]; **(C)** schematics of the combined PAM and OCT. PD: photodiode; HM: hot mirror; GM: 2D galvanometer; OBJ: objective lens; AMP: amplifier; UT: ultrasonic transducer; WT: water tank; SLED: superluminescent emitting diode; Ref: OCT reference arm. Reprinted with permission from [116].

It is clear that there are a diverse set of biomedical applications for a functional multimodal PAI-OCT system. The potential impact of such a broadly applicable technology has motivated the further investigation of possible multimodal system configurations. Here, depending on the photoacoustic imaging system, the multimodal PAI-OCT imaging systems are divided into three main categories of PAM-OCT, PAT-OCT, and PAE-OCT. The developed configurations for each category are reviewed, and their advantages and technical challenges are discussed.

Photoacoustic Microscopy Combined With Optical Coherence Tomography

One of the earliest works on the feasibility of multimodal PAM-OCT was demonstrated by Li et al. in 2009 [113]. Their proposed system operated in transmission mode and was only capable of imaging thin samples (**Figure 3A**). The reported penetration depth was ~1.5 and 1.8 mm for the PAM and OCT subsystems, respectively. Due to the mechanically translating objective, the system had slow acquisition time which highly limited its *in vivo* applications. Despite this limitation, the system was later used to look at the neovascularization of the mouse ear [114] (**Figure 3B**). Later Jiao et al. [115] developed a reflection-mode PAM-OCT system and imaged microvasculature of the mouse ear. The temporal resolution of their dual-modal system was limited by the pulse repetition rate of the PAM excitation source (~1 KHz). Liu et al. [116] developed a dual-modal system where a tunable dye laser was used as excitation source (**Figure 3C**). It leveraged the spectroscopic measurement capabilities of the PAM subsystem to evaluate total hemoglobin concentration as well as the metabolic rate of oxygen consumption in the mouse ear. Dual-modal PAM-OCT systems were further applied on various samples such as animal model of epilepsy progress [117], bovine cartilage osteoarthritis tissue [118], and imaging/needle guiding for injection and drug delivery in mouse thigh [104, 119].

Qin et al. [120] were among the first to develop the portable dual-modal PAM-OCT system. Their system was used for monitoring the recovery of an ulcer wound in the human lip. They carried out quantitative analysis by measuring total hemoglobin concentration as well as the size of the ulcer. *In vivo* images recorded from healing process of human lip ulcer are

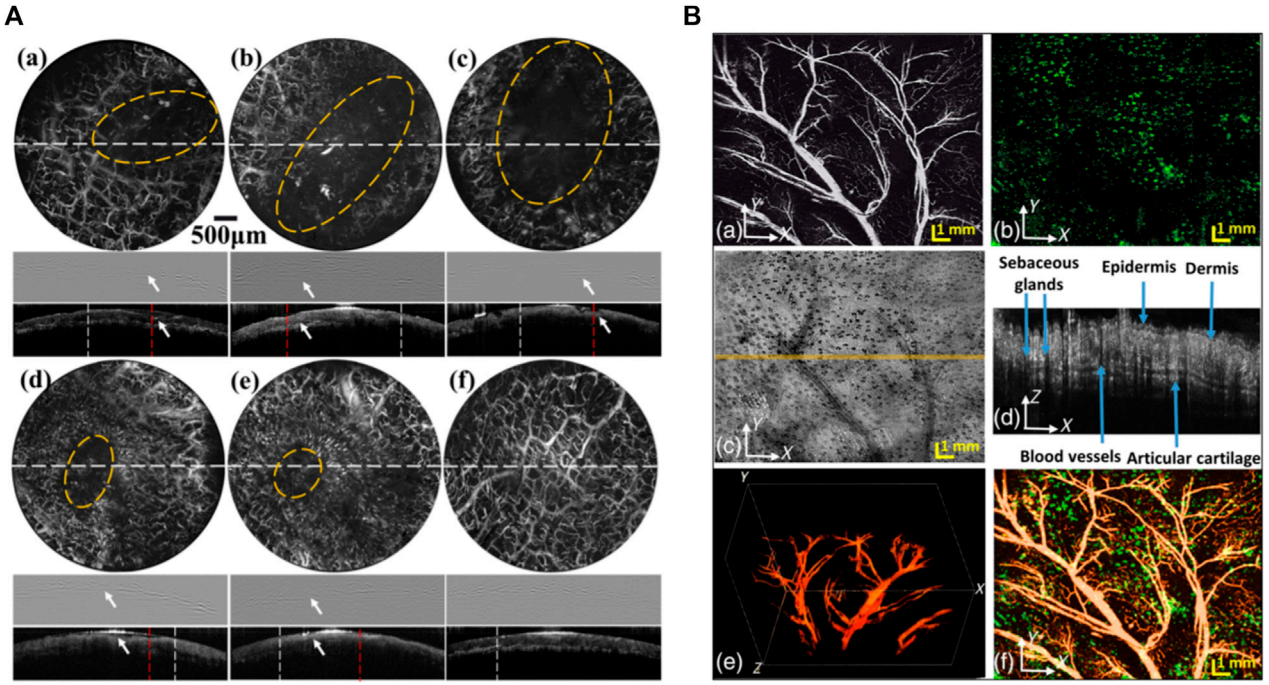

FIGURE 4 | (A) PAM and OCT results of the microvascular distribution and microstructures of the lower lip during the healing process of an ulcer wound. Row 1 in PAM images of the lip from day 1 to day 6. Row 2 PAM B-scans of the lip along the dashed white lines in Row1. Row3 OCT B-scans of the lip along the dashed white lines in Row1. The wounds are indicated by the yellow circles in PAM images and the white arrows in PAM B-scans. Scale bars: 500 μm. Reprinted with permission from [120]; **(B)** simultaneously acquired PAM, confocal microscopy (CFM), and OCT images of a mouse ear with dynamic focusing. **(A)** PAM image; **(B)** CFM image; **(C)** OCT images; **(D)** OCT B-scan at the location marked in panel; **(C)** by a solid line; **(E)** PAM 3-D image reconstruction; and **(F)** fused PAM projection and CFM images; bar: 1 mm. Reprinted with permission from [122].

shown in **Figure 4A**. The system offered lateral resolutions of ~8 μm for both modalities, and axial resolutions of 116.5 μm for PAM and 6.1 μm for OCT. However, since the system suffered from bulky size, in 2018 the same author demonstrated a handheld version of the system implemented with an MEMS-based optical scanner that offered more flexibility for oral tissue imaging [121]. The lateral resolutions of the system were improved to 3.7 μm for PAM and 5.6 μm for OCT, sufficient for visualizing morphological features and capillary loops in human oral tissue. Dadkhah et al. [122] took an additional step forward and developed a multimodal imaging system by integrating photoacoustic microscopy, OCT, and confocal fluorescence microscopy in one platform. The combination of optical and mechanical scanning together with dynamic focusing improved the sharpness and field of view of the images. The system achieved uniform resolution in a field-of-view of 12 mm × 12 mm with an imaging time of ~5 min for simultaneous *in vivo* imaging of the mouse ear (**Figure 4B**). The imaging speed of their system was limited by the pulse-repetition-rate of the PAM excitation laser.

In early 2020, Liu et al. [123] developed a dual-modal system in the NIR range for real-time, *in vivo* visualization of the tumor microenvironment changes during chemotherapy. The PAM subsystem utilized an optical parametric oscillation laser which had a wavelength range of 680–1,064 nm. The OCT subsystem was based on a commercial system with a center wavelength of ~1,300 nm, providing 12 μm axial resolution. This study worked to characterize tumor angiogenesis by monitoring changes in the vascular network's density, quantitative total hemoglobin concentration, and oxygen saturation of cancerous tissue. They suggested the dual-modal imaging-guided dose control system as a more efficient technology compared to the presently utilized tumor treatment options.

The majority of PAM-OCT configurations discussed earlier utilized ultrasound transducers for detecting acoustic waves. Despite offering high sensitivity, these transducers pose challenges when integrating PAM and OCT subsystems [124]. In transmission mode, the sample needs to be placed in a water tank or be in contact with ultrasound gel as a coupling medium [125–127], which limits the application of the technique to thin specimens. In reflection mode, because the opaque transducer obstructs the optical beam path, it needs to be positioned obliquely with respect to the optical axis which causes sensitivity loss [115, 128, 129]. In 2019, Hindl et al. [130] developed a reflection-mode OCT-PAM system using an all-optical akinetic Fabry–Perot etalon sensor. The miniature sensor included a rigid, fiber-based Fabry–Perot etalon with a transparent central opening and enabled linear signal detection over a broad bandwidth [131]. A schematic of the system is presented in **Figure 5A**. The OCT subsystem used a broadband laser centered at 840 nm, with a 5 μm axial resolution, and the PAM subsystem used a 532 nm pulsed laser operating at a pulse

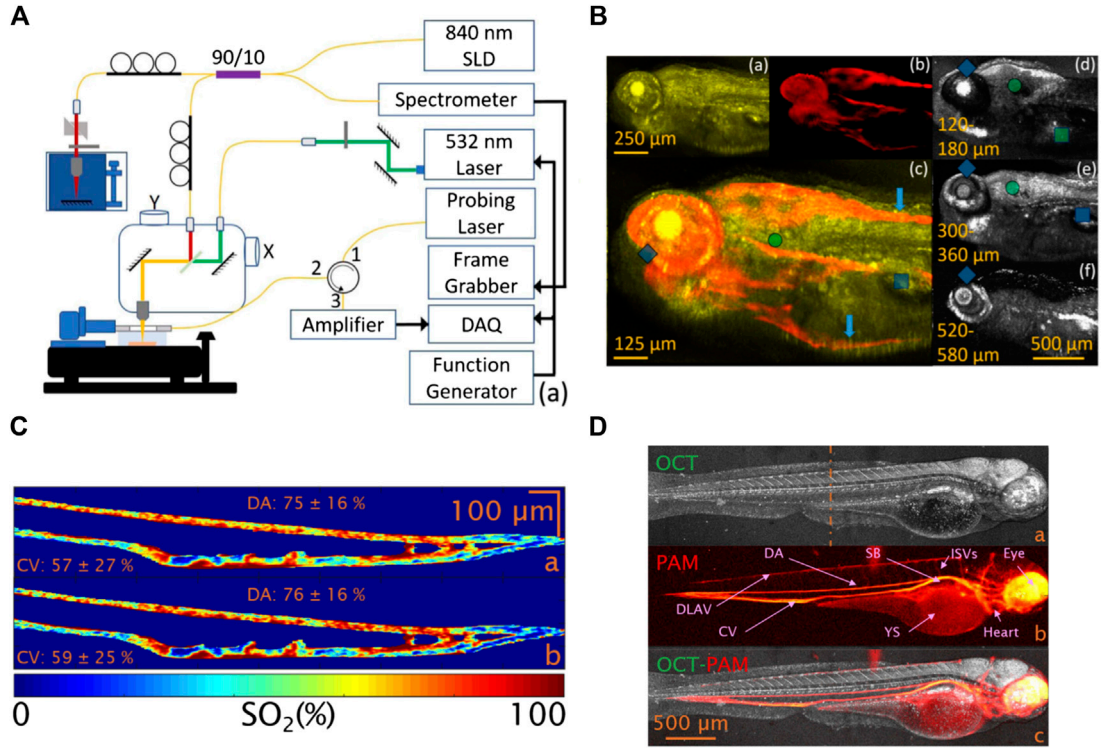

FIGURE 5 | (A) Schematic of the reflection-mode PAM-OCT system [130]; **(B)** images of a zebrafish larva. **(a)** OCT image; **(b)** PAM image; **(c)** color blended PAM-OCT image using **(a)** and **(b)**. **(d–f)** Images of OCT integrating 60 µm depth range. Reprinted with permission from [130]. **(C)** Oxygenation map of a zebrafish larval tail. The image is acquired after spectral unmixing using the absorption coefficients of human **(a)** and zebrafish blood **(b)**, respectively [132]. **(D)** OCT-PAM image of a zebrafish larva. **(a)** OCT average intensity projection, **(b)** PAM maximum amplitude projection, and **(c)** multimodal OCT-PAM. Reprinted with permission from [132].

repetition rate of 50 kHz. This system acquired OCT and PAM images sequentially. *In vivo* images of zebrafish larva's tissue and vascular morphologies are presented (**Figure 5B**). The system had limited imaging speed due to the use of stepper motors for scanning and the need for signal averaging to provide increased SNR. In addition, the OCT light source combined three superluminescent diodes which were not polarization aligned and resulted in various imaging artifacts and a degraded axial resolution. They recently reported a dual-modal system using a Ti:Sapphire broadband light source and fast laser scanning [132]. The axial resolution was 2.4 µm enabling visualization of retinal layers in the zebrafish model. Functional extensions of the PAM-OCT system including Doppler OCT and spectroscopic PAM were applied to monitor arterial pulsation and to measure absolute blood flow and oxygen saturation. The *in vivo* oxygenation measurement was acquired using a dye laser with a 10 KHz repetition rate at 578, 570, and 562 nm wavelengths. Representative images recorded using the system are presented in **Figure 5C&D**.

In the system configurations discussed earlier, both PAM and OCT subsystems used their own specific light source. Normally, PAM excitation is based on a narrowband pulsed laser, while OCT requires broadband, continuous light (e.g., superluminescent diode), or virtually continuous light (e.g., Ti: Sapphire laser). The other important difference in their light source is that OCT systems usually use near infrared (NIR) light for deeper penetration, but PAM mainly uses visible light to target the absorption peak of hemoglobin and melanin [133]. However, this apparent difference in wavelength, does not impede applying visible light for OCT or NIR light for PAM. Recent experiments have demonstrated applications of visible OCT for high-resolution imaging and measuring metabolic rate of oxygen for clinical studies [134, 135], while NIR light has been used for imaging lipid and collagen tissues in PAM [136–138]. Several studies explored the feasibility of using a single light source for PAM excitation and OCT imaging, which would reduce the complexity and costs of the system; in addition, it will generate synchronized and coregistered PAM and OCT images. Zhang et al. [14] demonstrated the first single pulsed light source for PAM-OCT in 2012 and termed the technique optical coherence photoacoustic microscopy (OC-PAM). Experimental setup of the proposed system is demonstrated in **Figure 6A**. The system was in transmission mode with a custom-designed broadband dye laser centered at 580 nm with 20 nm bandwidth, and a 5 KHz pulse repetition rate. The system was tested on the *in vivo* mouse ear, and promising results were demonstrated; however, the low repetition rate of the light source limited the imaging speed, and the noisy spectrum of the laser degraded the quality of OCT images. Due to their broad spectral bandwidth, supercontinuum (SC) sources were employed in OC-

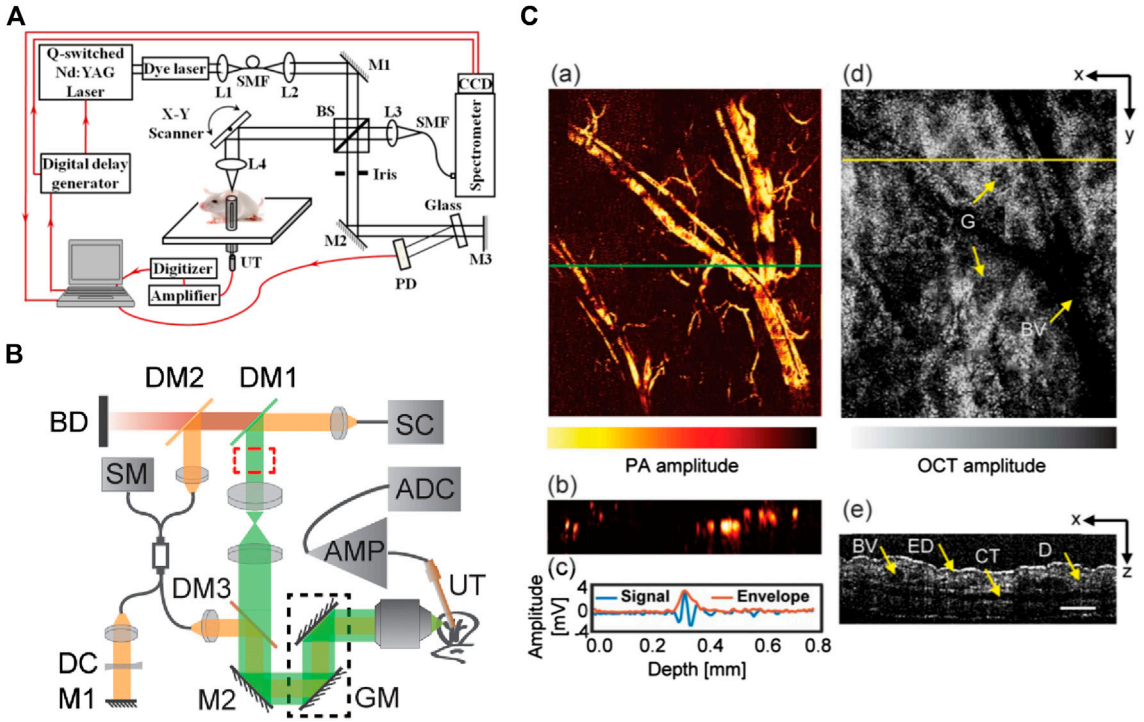

FIGURE 6 | (A) Schematic of the experimental system of a free-space OC-PAM. BS, beam splitter; SMF, single-mode fiber; PD, photodiode; UT, ultrasonic transducer; L, lens, M, mirror. Reprinted with permission from [14]. **(B)** Schematic of PAM-OCT system setup. SC, supercontinuum; DM, dichroic mirrors; GM, galvanometer; UT, ultrasound transducer; AMP, amplifier; ADC, digitizer; SM, spectrometer; DC, dispersion compensating slab; M, mirrors; BD, beam dump. Reprinted with permission from [129]. **(C)** Results of *in vivo* mouse ear imaging. **(a)** En-face PAM image; **(b)** PAM B-scan taken from location indicated by the green line in **(a)**. **(c)** Typical PA A-line and its signal envelope obtained by a Hilbert transform. **(d)** En-face OCT image. G, gland; BV, blood vessel. **(e)** OCT B-scan taken from location indicated by yellow line in **(d)**. ED, epidermis; CT, cartilage; D, dermis. Scale bar, 150 μm. Reprinted with permission from [129].

PAM systems as well [125, 139]. In 2016, Shu et al. [129] reported a dual-modality OC-PAM system using a homebuilt fiber-based SC source (**Figure 6B**). The beam coming from the light source was split into a shorter wavelength band (500–800 nm) for PAM and a longer wavelength band (800–900 nm) for OCT. The system was tested for *in vivo* imaging of the mouse ear, and multispectral PAM was performed on the *ex vivo* porcine retinal sample (**Figure 6C**).

Photoacoustic Microscopy Combined With Optical Coherence Tomography for Ophthalmic Applications

One of the few and important applications that developed dual-modal PAM-OCT systems have explored so far is ophthalmic imaging. Due to the prevalence of OCT imaging for clinical ophthalmology, dual-modal PAM-OCT is a natural extension for imaging the eye. In ophthalmic application, access to the absorption information could provide information about the functional and molecular properties of the tissue, such as evaluating the retinal pigment epithelium in diseases such as age-related macular degeneration or measuring metabolic rate of oxygen in retinal and choroidal circulations in diabetic retinopathy. In 2010, Jiao et al. [140] reported one of the first multimodal PAM-OCT ophthalmoscopes which used an unfocused transducer directly placed on the sclera. The OCT subsystem was based on an SD-OCT design consisting of a superluminescent diode centered at 870 nm. Experimental results were demonstrated for *in vivo* imaging of retinal vessels and the retinal pigment epithelium layer in rat eyes, with a laser pulse energy well within the ANSI safety limits. Song et al. [141] further extended this system to include additional modalities such as scanning laser ophthalmoscopy and fluorescein angiography and imaged rat retina. They also measured the metabolic rate of oxygen in rat retina [90]. **Figure 7** illustrates the developed functional imaging system and the combined PAM and OCT scanning pattern on the retina. In 2015, Liu et al. [142] developed an OC-PAM system by using a single pulsed broadband light source with a central wavelength of 800 nm. Since the absorption coefficient of hemoglobin is relatively weak at this wavelength, the PAM signals were mainly providing melanin-specific information of the retina. The imaging speed of the system was limited by the 10 KHz pulse repetition rate of the light source, which is not as high as conventional ophthalmic OCT systems. To avoid possible motion artifacts and image blurring/disruption, high imaging speed is required. Robinson et al. [143] reported that the eye has a fixation time of ~500 ms. Increasing the repetition rate can improve the imaging speed; however, it will also increase the average power of the light source which is

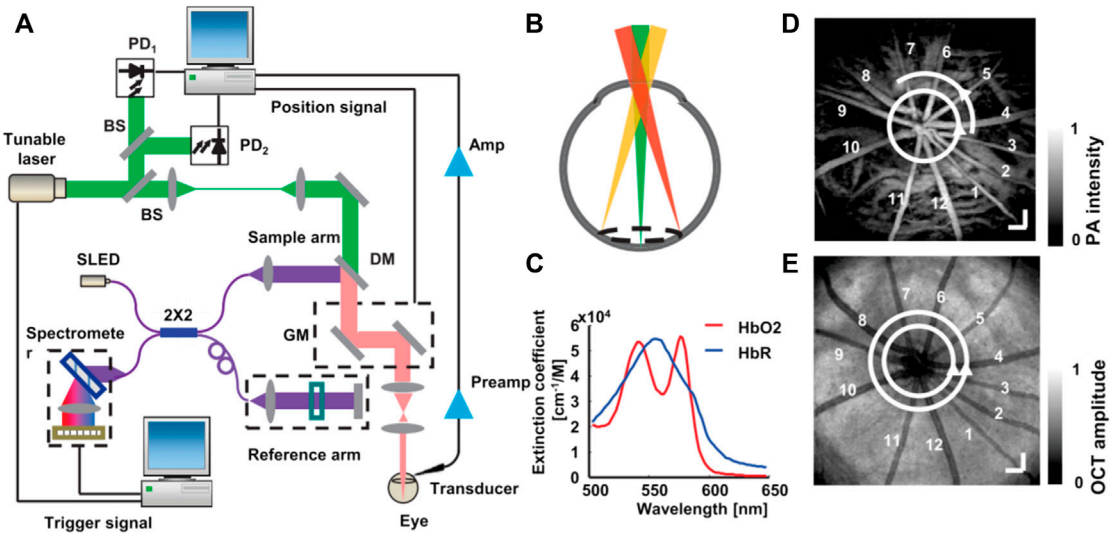

FIGURE 7 | Illustration of integrated PAM and SD-OCT to measure retinal metabolic rate of oxygen. **(A)** Schematic of the experimental setup; **(B)** circular scanning pattern on the retina; **(C)** molar extinction coefficient spectrum of oxy- and deoxyhemoglobin; **(D)** a maximum-amplitude-projection PAM fundus image showing major retinal vessels. Bar: 200 mm; **(E)** an OCT fundus image of the same rat showed in the panel **(D)**. Bar: 200 mm. Reprinted with permission from [90].

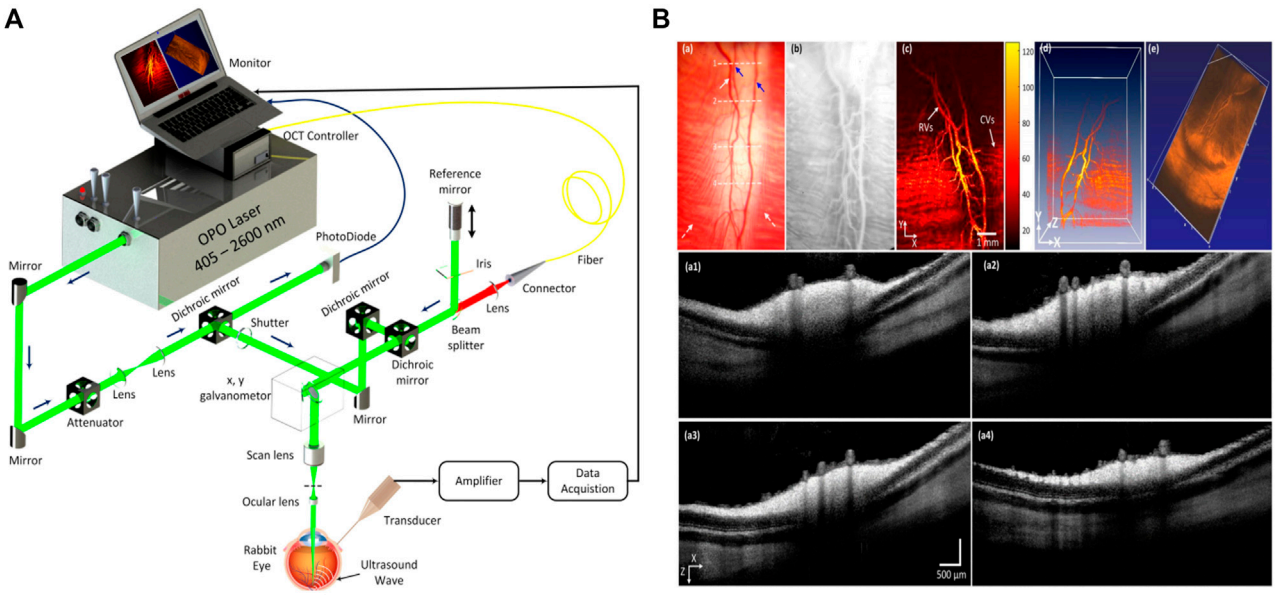

FIGURE 8 | (A) Schematic diagram of the integrated PAM and OCT systems for multimodal retinal imaging. Reprinted with permission from [147]; **(B)** images of retinal blood vessels in rabbits: **(a)** color fundus photography of retina. **(b)** Fluorescein angiography image showing retinal and choroidal capillaries. **(c)** Corresponding maximum amplitude projection PAM images of retina; **(d,e)** volumetric PAM and OCT image, respectively. **(a1–a4)** Cross-sectional OCT images acquired along the scanning lines from **(a)**. Reprinted with permission from [148].

constrained by existing laser safety limits. This may cause issues in practical applications where there are pulses overlapping in the retina. This highlights the trade-off between pulse repetition rate and pulse energy. Developing a highly sensitive PA detection method is the key for reducing the pulse energy and thus making it safe for clinical eye imaging.

Mice and rat eye models have been extensively used in preclinical ophthalmic imaging experiments. The eyeballs of these animals are smaller (axial length of mouse eyeballs ~3 mm, rats ~6 mm) compared to humans (~25 mm). Therefore, using animals with larger eyeballs, such as rabbits and monkeys, could help benefit ophthalmic studies. Tian et al.

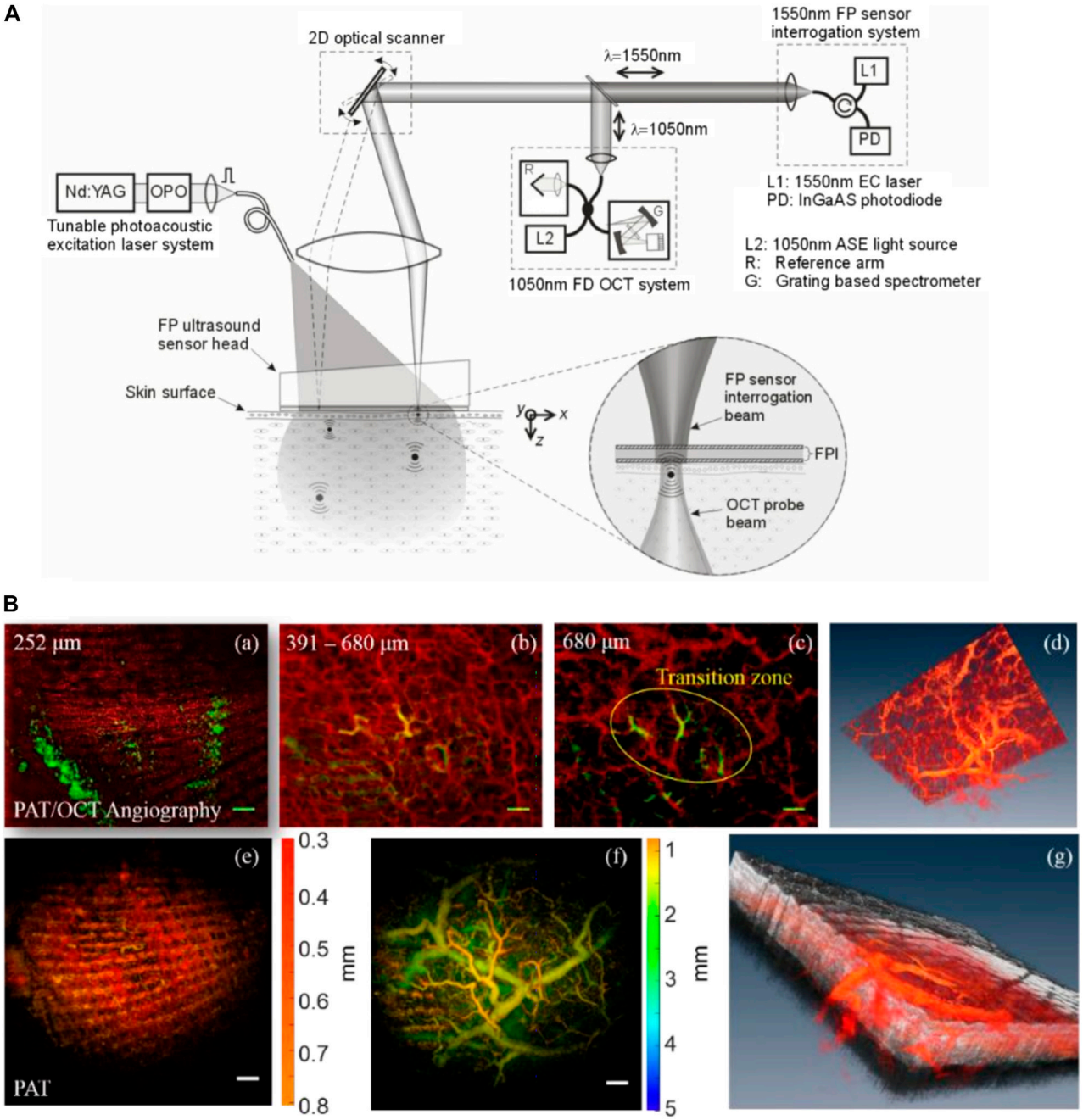

FIGURE 9 | (A) Dual-modal PAT-OCT scanner. Reprinted with permission from [151]. **(B) (a–c)** overlaid PAT-OCTA images with PAT in the green channel and OCTA in the red channel. **(d)** Blood vessel network given in volumetric display by fused OCTA and PAT data. **(e)** PAT image. **(f)** PAT image in deeper region. **(g)** A snapshot of the 3D volume with OCT in gray, OCTA, and PAT in red color map. Scale bar = 1 mm. Reprinted with permission from [153].

[144] were among the first groups to demonstrate the application of the PAM-OCT system for chorioretinal imaging of rabbits in 2017. They were able to visualize depth-resolved retinal and choroidal vessels using laser exposure well below the ANSI safety limit. A multimodal imaging system combining PAM, OCT, and florescence microscopy was demonstrated by Zhang et al. [145, 146], and it was applied to evaluate angiogenesis in both albino and pigmented live rabbit eyes. The authors claimed that in pigmented rabbits, melanin from the retinal pigment epithelium overlies the choroid and thus possibly blocks the diffuse choroidal hyperfluorescence and improve the image quality of all the three modalities. Nguyen et al. [95] employed gold nanoparticles as a contrast agent for both OCT and PAM imaging. They imaged *in vivo* rabbit retina, and the exogenous

contrast agent improved the efficiency for visualizing capillaries, and retinal and choroidal vessels. The speed of the system was defined by 1 KHz pulse repetition rate of the excitation laser. The system was later used to evaluate optical properties of retinal vein occlusion and retinal neovascularization in living rabbits [147]. Spectroscopic PAM was performed at wavelengths ranging from 510 to 600 nm to further evaluate dynamic changes in the retinal morphology [148]. The schematic of the developed system and recorded images using the multimodal system are presented in **Figure 8A B**, respectively.

In general, PAM devices have relatively low axial resolution compared to OCT systems, and there is a large resolution gap between two modalities. Unlike, OCT, whose axial resolution is defined by the spectral bandwidth of the light source in PAM axial resolution, depends on the detector's bandwidth and ultrasound attenuation [33]. The typical axial resolution of OCT systems is less than 10 μm, which corresponds to ~100 MHz ultrasound signal frequency. These high-frequency signals can hardly survive in some cases where the distance from the source to the detector is long such as retina imaging. Therefore, for ophthalmic PAM-OCT, it is importance to enhance PA detection mechanism to reduce the gap in axial resolution.

Photoacoustic Tomography Combined With Optical Coherence Tomography

Due to the high penetration depth benefits, dual-modal PAT-OCT systems are mainly used for applications where depth information is required [108, 149]. For example, in dermatology, while OCT techniques visualize superficial small capillary loops with vessel diameters from 10 to 200 μm to a depth of 1 mm, PAT enables visualization of vasculatures with diameters from 100 μm down to a depth of several centimeters. Therefore, the combination of these modalities could provide a complete perfusion map of the skin [150]. In addition, acquiring PAT and OCT images from overlapping or identical regions has the advantage that highly absorbing structures, which appear as shadow in OCT images (e.g., blood vessels), can be observed in PAT images [16].

In 2011, Zhang et al. [151] developed a PAT-OCT system and demonstrated *in vivo* volumetric images of vasculature and surrounding tissue in mouse and human skin. The schematic of their system is presented in **Figure 9A**. The system employed an integrated all-optical detection scheme for both modalities in reflection-mode maintaining a field of view of ~13 mm × 13 mm. The photoacoustic waves were detected using a Fabry–Perot sensor place on the surface of the skin. The planar-view PAT system based on the Fabry–Perot interferometer is of particular interest in most dual-modal PAT-OCT applications because of the simplicity of sample positioning and optical detection mechanism [149, 152]. The study reported tissue information of vascular structure to a depth of ~5 mm. Similar systems were further developed, and *in vivo* clinical experiments were performed on healthy and pathological skin [103, 153–156] (**Figure 9B**). Initial clinical studies demonstrate that the dual-modal PAT-OCT systems hold a great potential for applications in dermatology [157]. Recently, Liu et al. [108] published a comprehensive overview of the dual-modality PAT-OCT system in the field of dermatology and the challenges and prospects of these two imaging modalities for dermatology were discussed thoroughly.

Photoacoustic Endoscopy Combined With Optical Coherence Tomography

Toward realizing dual-modality PAE-OCT, in 2011 Yang et al. [158] made the initial step by integrating ultrasound tomography with photoacoustic and OCT imaging in a single intraoperative probe. The performance of the system was demonstrated on *ex vivo* porcine and human ovaries. The OCT subsystem used a swept-source laser centered at ~1,300 nm with 110 nm spectral bandwidth and a 20 KHz scan rate, and the PAE subsystem had a tunable Ti: Sapphire laser with a spectral range of 700–950 nm and a 15 Hz repetition rate. The ultrasound transducer operated as both PAI detection and ultrasound transmission and detection. **Figure 10A** depicts the combined three-modality endoscopic probe. The overall diameter of the endoscope was 5 mm and included a ball-lensed OCT sample arm probe, and a multimode fiber to deliver light for photoacoustic imaging. Later, in 2013, Xi et al. [159] reported an endoscopic delivery probe with a diameter of 2.3 mm. The system had a low-frequency unfocused 10 MHz transducer for photoacoustic signal detection and a time-domain OCT system at 1 kHz. The performance of their system could be improved in several ways such as increasing the central frequency of photoacoustic transducer, employing a higher-resolution DAQ card, and replacing the time-domain OCT device with a frequency-domain OCT device to enhance the sensitivity. Inspired by one of the initial efforts in the field (Yang et al. [158] study), Dai et al. [160] developed a multimodal miniature probe through which OR-PAM, OCT, and pulsed-echo ultrasound images were acquired coaxially and were displayed simultaneously. **Figure 10B** depicts the schematic of the integrated miniature probe. The 2 mm diameter probe had a 40 MHz unfocused ultrasound transducer for both OR-PAM detection and ultrasound transmission and receiving, and *in vivo* images of the rat ear were recorded (**Figure 10C**). The results show cross-sectional images acquired by OR-PAM, OCT, ultrasound, and combined images, corresponding to the three dashed lines in the respective maximum-amplitude-projection image. Despite offering high imaging resolution, the system suffered from lack of rotational scanning and its imaging speed was limited by the slow repetition rate (20 Hz) of the pulsed laser. Mathews et al. [161] developed a dual-modal intravascular imaging probe using a commercial OCT catheter and a fiber optic ultrasound sensor based on Fabry–Perot cavity. Their experimental setup and the enlarged view of the distal end of the probe is presented in **Figure 10D**. They demonstrated circumferential PAE-OCT imaging and multispectral PAI on a synthetic phantom. One limitation of their probe configuration was that the stationary fiber optic ultrasound receiver resulted in shielding of the photoacoustic waves by the OCT catheter for certain excitation angles. As a result, the detected photoacoustic signal amplitude varied relatively with respect to the receiving

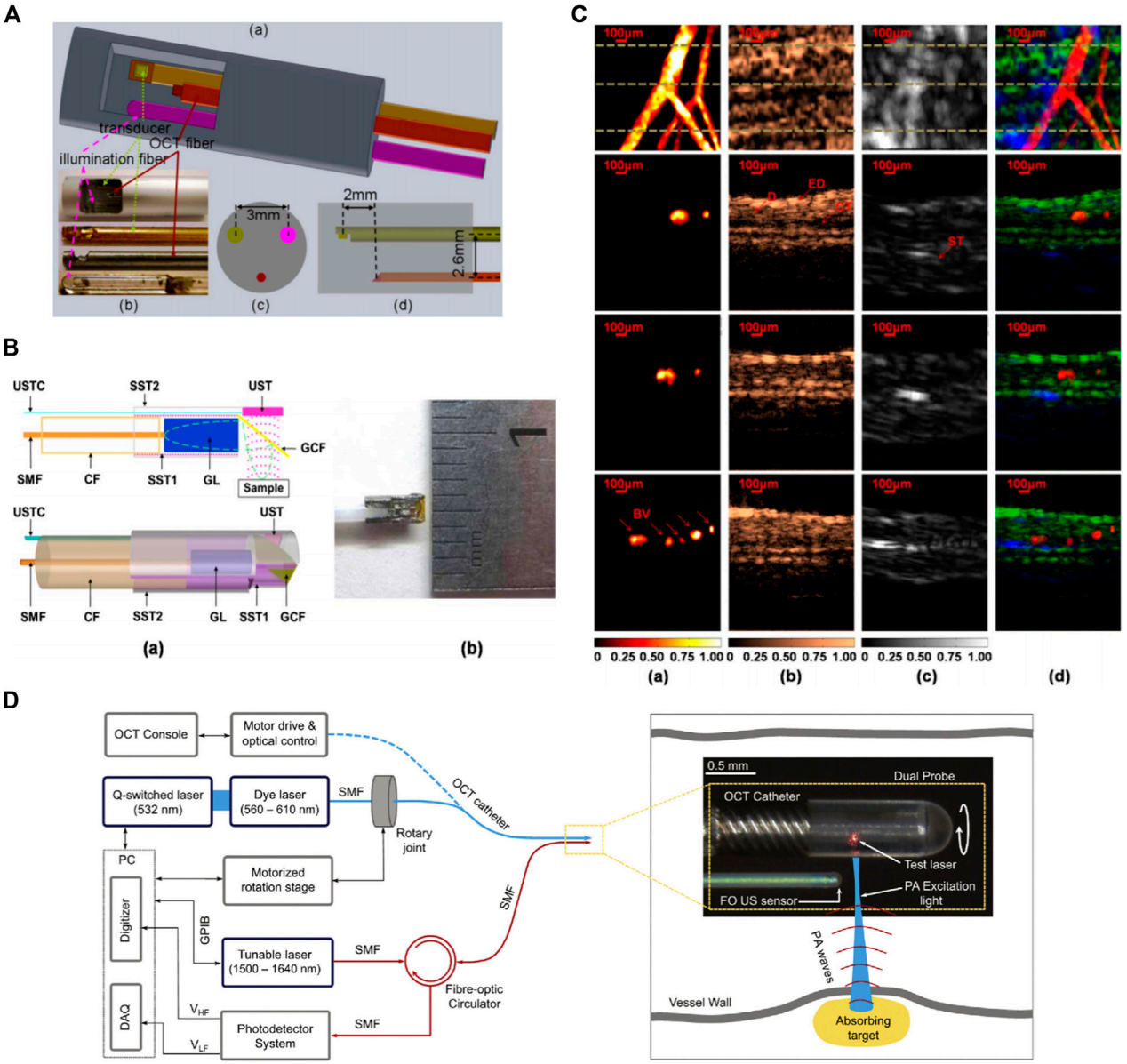

FIGURE 10 | (A) Integrated OCT-US-PAI three-modality endoscopic probe. Reprinted with permission from [158]. **(B)** Schematic and photograph of miniature integrated probe. Reprinted with permission from [160]. **(C)** *In vivo* images of a rat ear. Maximum amplitude projection images (top row) and cross-sectional images (2nd, 3rd, and bottom rows) corresponding to the dotted lines in first row images. **(a)** OR-PAM, **(b)** OCT, **(c)** US, and **(d)** fused images. Reprinted with permission from [160]. **(D)** Schematic of the dual-modality PA-OCT system. An enlarged image of the distal end of the probe. Reprinted with permission from [161].

angle in the rotation plane. In general, future direction for multimodal PAE-OCT studies can be focused on improving scanning speed, miniaturizing the probe size, and enhancing detection mechanism.

DISCUSSION

The combination of PAI and OCT has drawn a large amount of research interest throughout the past decade. This multimodal technology has the potential to provide chromophore selective image contrast in concert with depth-resolved scattering contrast. Despite offering several advantages, there are still a couple of key challenges to overcome.

One of the major limitations of current systems is the significant imaging speed mismatch between OCT and PAI subsystems. Imaging speed is a critical parameter when it comes to real-time functional studies. Additionally, faster imaging speeds will help systems mitigate image artifacts due to involuntary motion. Thanks to technological developments,

current OCT systems are able to reach video rate over a large scanning area [162–164]. The same is not true for PAI systems, and as a result, the imaging speed of the dual-modal system is defined by the pulse repetition rate of the PA excitation light source or mechanical scanning speed of the PAI probe head. Widespread implementation of PAI-OCT systems will depend on the development and integration of suitable light sources with high repetition rate, stable short pulse illumination, and high output energy at multiple wavelengths. This development would enable PAI-OCT systems to capture real-time large field-of-view images.

The other major constraint in most PAI systems is that most ultrasound detectors are opaque. Therefore, the physical size of the sensor obstructs the optical path required for OCT acquisition. To overcome this limitation, in some studies the active size of the transducer was reduced, or the transducer was positioned obliquely [131]. However, since the sensitivity of the photoacoustic imaging scales with the active element size of the detector, these methods effect the sensitivity of the photoacoustic images and will degrade image quality [165]. Several studies have investigated optimizing light delivery to improve PA image contrast and signal-to-noise ratio [166–168]. Monte Carlo simulations suggest that the optimal PA illumination depends on the optical properties of the sample [169]. Improvements in light delivery have also be investigated through using optically transparent spacer between the transducer and sample to directly deliver light to the surface underneath the transducer [170–172]. In addition, custom transducers and new materials have been explored to develop different illumination geometries and improve the quality of the PA image [173, 174]. However, these methods require significant modification of the system and cannot be readily integrated into standard clinical scanners [175].

Another important constraint of ultrasound transducers used in most PAI systems rises from their need for physical contact with the sample through a coupling medium. This contact-based detection minimizes the acoustic reflection losses at poorly matched interfaces such as tissue and air. However, it is not suitable for several clinical and preclinical applications such as wound assessment, brain imaging, or ophthalmic imaging [176]. Various approaches have been suggested to overcome this limitation among which optical detection approaches hold the promise to provide high sensitivity over a wide frequency range [177–180]. Optical detection methods also offer the opportunity of developing miniaturized and optically transparent ultrasound detectors [181]. The pure optical PAI-OCT system is more attractive nowadays and offers a better choice for the multimodal imaging. Different studies have been conducted on the performance of pure optical photoacoustic imaging integrated with optical coherence tomography [182, 183]. In [119], authors proposed a resolution-matched reflection-mode PAM-OCT system for *in vivo* imaging applications. The PAM subsystem is based on a polarization-dependent reflection ultrasonic detection (PRUD), which still requires water as a coupling medium and complicated optical alignment. The akinetic sensor employed in [130] is another example of the pure optical PA detection sensor, which also suffers from the need for acoustic gel as a coupling medium. All-optical PA detection methods have been investigated for noncontact, dual-modal PAI-OCT system as well. These methods include homodyne interferometer [85], heterodyne interferometer [184], and two-wave mixing interferometer [185]. These methods are mainly based on detection of surface vibrations induce by photoacoustic pressure waves. While they bring noncontact PA imaging into the field, detecting surface vibrations using an interferometer requires high phase stability. Thus, to maintain these interferometric PA detection systems at their highest sensitivity, complicated phase stabilization techniques are required. In addition, the success of the methods relies on surface topography and has difficulty while applied to uneven surfaces or *in vivo* applications where motion is undeniable. Recent advances in noninterferometric photoacoustic remote sensing (PARS) have proved the potential of technique for various imaging applications [186–190]. Martell et al. [191] have reported all-optical, noncontact, dual-modal PARS-OCT and discussed the potential of the system for different *in vivo* applications.

As a hybrid imaging modality, PAI-OCT imaging combines naturally complimentary advantages of photoacoustic imaging and optical coherence tomography. Despite the aforementioned technical challenges, the possible impact of a PAI-OCT to many biomedical applications explored in this paper warrants significant further investigation. With the continued advancements of new detection methods, along with new light sources, multimodal PAI-OCT imaging has a promising future in biomedical imaging as a powerful tool for diagnostics.

AUTHOR CONTRIBUTIONS

ZH compiled the article and prepared figures, JS edited parts of the article, and PR was the principle investigator, set the article scope, and proofread the article.

FUNDING

New Frontiers in Research Fund–Exploration (NFRFE-2019-01012); Natural Sciences and Engineering Research Council of Canada (DGECR-2019-00143, RGPIN2019-06134); Canada Foundation for Innovation (JELF #38000); Mitacs (IT13594); Center for Bioengineering and Biotechnology (CBB Seed fund); University of Waterloo; illumiSonics (SRA #083181).

ACKNOWLEDGMENTS

The authors acknowledge funding from the University of Waterloo, NSERC Discovery grant, MITACS accelerator program, Canada Foundation for Innovation (CFI-JEFL), Center for Bioengineering and Biotechnology seed funding, New Frontiers in Research Fund–exploration, and research partnership support from illumiSonics Inc.

REFERENCES

1. Tempany CM, Jayender N, Kapur A, Bueno R, Golby T, Agar J, et al. Multimodal imaging for improved diagnosis and treatment of cancers. *Cancer* (2015) 121(6):817–27. doi:10.1002/cncr.29012
2. JoleszJayender M, Shu J. Multimodal molecular imaging: current status and future directions. *Contrast Media Mol Imag*. (2018) 2018, 1382183. doi:10.1155/2018/1382183
3. Rodríguez-Palomares JF, García Fernández MA, Barba Cosials J. Integrating multimodal imaging in clinical practice: the importance of a multidisciplinary approach. *Rev Esp Cardiol*. (2016) 69(5):477–9. doi:10.1016/j.rec.2016.01.019
4. Pan H, Myerson J, Yang X, Lanza G, Wickline SA. Atherosclerosis endothelial activation quantification *in vivo* with fluorine magnetic resonance imaging and spectroscopy. *J Cardiovasc Magn Reson* (2014) 16(1):O91. doi:10.1186/1532-429X-16-S1-O91
5. Bruckman MA, Jiang K, Simpson MJ, Randolph LN, LuytL G, Steinmetz NF. Dual-modal magnetic resonance and fluorescence imaging of atherosclerotic plaques *in vivo* using VCAM-1 targeted tobacco mosaic virus. *Nano Lett*. (2014) 14(3):1551–8. doi:10.1021/nl404816m
6. O'HalloranJiang R, Kopell BH, Sprooten E, Goodman WK, Frangou S. Multimodal neuroimaging-informed clinical applications in neuropsychiatric disorders. *Front Psychiatr*. (2016) 7:63. doi:10.3389/fpsyt.2016.00063
7. Teipel S, Drzezga A, Grothe MJ, Barthel H, Chételat G, Schuff N, et al. Multimodal imaging in Alzheimer's disease: validity and usefulness for early detection. *Lancet Neurol* (2015) 14(10):1037–53. doi:10.1016/S1474-4422(15)00093-9
8. FellgiebelDrzezga MF, Zerda A, Jokerst JV, Zavaleta CL, Kempen PJ, Mittra E, Pitter K, et al. A brain tumor molecular imaging strategy using a new triple-modality MRI-photoacoustic-Raman nanoparticle. *Nat Med* (2012) 18(5):829–34. doi:10.1038/nm.2721
9. Gambhirde la Zerda J, Wang LV. Photoacoustic microscopy. *Laser Photon Rev*. (2013) 7(5):758–78. doi:10.1002/lpor.201200060
10. Wang LV, Hu S. Photoacoustic tomography: in vivo imaging from organelles to organs. *Science*. (2012) 335(6075):1458–62. doi:10.1126/science.1216210
11. Tan ACS, Tan GS, Denniston AK, Keane PA, Ang M, Milea D, et al. An overview of the clinical applications of optical coherence tomography angiography. *Eye* (2018)32(2). doi:10.1038/eye.2017.181
12. Kashani AH, Chen CL, Gahmc JK, Zheng F, Richtera GM, Rosenfeld PJ, et al. Optical coherence tomography angiography: a comprehensive review of current methods and clinical applications. *Prog Retin Eye Res* (2017) 60:66–100. doi:10.1016/j.preteyeres.2017.07.002
13. WangChen AM, Nguyen FT, Oldenburg AL, Marks DL, Boppart SA. Optical coherence tomography: a review of clinical development from bench to bedside. *J Biomed Optic*. (2007) 12(5):051403. doi:10.1117/1.2793736
14. Boppart X, Zhang HF, Jiao S. Optical coherence photoacoustic microscopy: accomplishing optical coherence tomography and photoacoustic microscopy with a single light source. *J Biomed Optic*. (2012) 17(3):030502. doi:10.1117/1.JBO.17.3.030502
15. Brunker J, Yao J, Laufer J, Bohndiek SE. Photoacoustic imaging using genetically encoded reporters: a review (2017). Available at: https://www-spiedigitallibrary-org.proxy.lib.uwaterloo.ca/journals/journal-of-biomedical-optics/volume-22/issue-07/070901/Photoacoustic-imaging-using-genetically-encoded-reporters-a-review/10.1117/1.JBO.22.7.070901.full (Accessed June 17, 2020).
16. Drexler W, Fujimoto JG. *Optical coherence tomography: technology and applications*. AG Switzerland: Springer Science & Business Media (2008). 1346 p.
17. Wang LV. Multiscale photoacoustic microscopy and computed tomography. *Nat Photon*. (2009) 3(9):503–9. doi:10.1038/nphoton.2009.157
18. Wang LV, Hu S. Photoacoustic tomography: in vivo imaging from organelles to organs. *Science*. (2012) 335(6075):1458–62. doi:10.1126/science.1216210
19. Bell AG. On the production and reproduction of sound by light. *In Proc Am Assoc Adv Sci*. (1881) 29:115–36. doi:10.2475/ajs.s3-20.118.305
20. Wang LV, Wu H-I. *Biomedical optics: principles and imaging*. Hoboken, NJ: John Wiley & Sons, Inc. (2009). p 376.
21. Beard P. Biomedical photoacoustic imaging. *Interface Focus*. (2011) 1(4):602–31. doi:10.1098/rsfs.2011.0028
22. Chan J, Zheng Z, Bell K, Le M, Reza PH, Yeow JT. Photoacoustic imaging with capacitive micromachined ultrasound transducers: principles and developments. *Sensors*. (2019) 19(16):3617. 10.3390/s19163617
23. Bowen T. Radiation-Induced thermoacoustic soft tissue imaging. In: 1981 ultrasonics symposium; 1981 October 14–16; Chicago, IL. IEEE (1981). p. 817–22.
24. Kolkman RGM, Hondebrink E, Steenbergen W, de Mul FFM. *In vivo* photoacoustic imaging of blood vessels using an extreme-narrow aperture sensor. *IEEE J Sel Top Quant Electron*. (2003) 9(2):343–6. doi:10.1109/JSTQE.2003.813302
25. Hajireza P, Sorge J, Brett M, Zemp R. *In vivo* optical resolution photoacoustic microscopy using glancing angle-deposited nanostructured Fabry-Perot etalons. *Opt Lett*. (2015) 40(7):1350–3.doi:10.1364/OL.40.001350
26. Xia J, Chatni MR, Maslov K, Guo Z, Wang K, Anastasio M, et al. Whole-body ring-shaped confocal photoacoustic computed tomography of small animals *in vivo*. *J Biomed Optic*. (2012) 17(5):050506. doi:10.1117/1.JBO.17.5.050506
27. WangChatni L, Hu P, Shi J, Appleton CM, Maslov K, Li L, et al. Single-breath-hold photoacoustic computed tomography of the breast. *Nat Commun*. (2018) 9(1):2352. doi:10.1038/s41467-018-04576-z
28. WangHu CL, Luke GP, Emelianov SY. Photoacoustic imaging for medical diagnostics. *Acoust Today*. (2012) 8(4):15. doi:10.1121/1.4788648
29. Stein EW, Maslov K, Wang LV. Noninvasive, *in vivo* imaging of blood-oxygenation dynamics within the mouse brain using photoacoustic microscopy. *J Biomed Optic*. (020502200) 14(2):020502. doi:10.1117/1.3095799
30. Yao J, Wang LV. Photoacoustic microscopy. *Laser Photon Rev*. (2013) 7(5):758–78. doi:10.1002/lpor.201200060
31. Hu S, Wang LV. Photoacoustic imaging and characterization of the microvasculature. *J Biomed Optic*. (2010) 15(1):011101. doi:10.1117/1.3281673
32. Guo H, Li Y, Qi W, Xi L. Photoacoustic endoscopy: a progress review. *J Biophot*. n/a:e202000217. doi:10.1002/jbio.202000217
33. Yao J, Wang LV. Sensitivity of photoacoustic microscopy. *Photoacoustics*. (2014) 2(2):87–101. doi:10.1016/j.pacs.2014.04.002
34. Hu S. Emerging concepts in functional and molecular photoacoustic imaging. *Curr Opin Chem Biol*. (2016) 33:25–31. doi:10.1016/j.cbpa.2016.04.003
35. Moothanchery M, Pramanik M. Performance characterization of a switchable acoustic resolution and optical resolution photoacoustic microscopy system. *Sensors*. (2017) 17(2):357. doi:10.3390/s17020357
36. Zhang C, Maslov K, Wang LV. Subwavelength-resolution label-free photoacoustic microscopy of optical absorption *in vivo*. *Opt Lett*. (2010) 35(19):3195. doi:10.1364/OL.35.003195
37. Li M, Tang Y, Yao J. Photoacoustic tomography of blood oxygenation: a mini review. *Photoacoustics*. (2018) 10:65–73. doi:10.1016/j.pacs.2018.05.001
38. Yao J, Maslov KI, Shi Y, Taber LA, Wang LV. *In vivo* photoacoustic imaging of transverse blood flow by using Doppler broadening of bandwidth. *Opt Lett*. (2010) 35(9):1419–21. doi:10.1364/OL.35.001419
39. Yao J, Wang LV. Transverse flow imaging based on photoacoustic Doppler bandwidth broadening. *J Biomed Optic*. (2010) 15(2):021304. doi:10.1117/1.3339953
40. Yao J, Ke H, Tai S, Zhou Y, Wang LV. Absolute photoacoustic thermometry in deep tissue. *Opt Lett*. (2013) 38(24):5228–31. doi:10.1364/ol.38.005228
41. Gao L, Wang L, Li C, Liu Y, Ke H, Zhang C, et al. Single-cell photoacoustic thermometry. *J Biomed Optic*. (2013) 18(2):26003. doi:10.1117/1.JBO.18.2.026003
42. WangWang P, Forbrich A, Zemp R. *In-Vivo* functional optical-resolution photoacoustic microscopy with stimulated Raman scattering fiber-laser source. *Biomed Optic Express*. (2014) 5(2):539. doi:10.1364/BOE.5.000539
43. Yao J, Wang L, Yang TT, Maslov KI, Wong JM, Li L, et al. High-speed label-free functional photoacoustic microscopy of mouse brain in action. *Nat Methods*. (2015) 12(5):407–10. doi:10.1038/nmeth.3336
44. Chen Z, Rank E, Meiburger KM, Sinz C, Hodul A, Zhang E, et al. Non-invasive multimodal optical coherence and photoacoustic tomography for human skin imaging. *Sci Rep*. (2017) 7(1):17975. doi:10.1038/s41598-017-18331-9
45. Laufer J, Zhang E, Raivich G, Beard P. Three-dimensional noninvasive imaging of the vasculature in the mouse brain using a high resolution photoacoustic scanner. *Appl Optic*. (2009) 48(10):D299–306. doi:10.1364/ao.48.00d299

46. Paproski RJ, Heinmiller A, Wachowicz K, Zemp RJ. Multi-wavelength photoacoustic imaging of inducible tyrosinase reporter gene expression in xenograft tumors. *Sci Rep*. (2014) 4:5329. doi:10.1038/srep05329
47. Sethuraman S, Amirian JH, Litovsky SH, Smalling RW, Emelianov SY. *Ex vivo* characterization of atherosclerosis using intravascular photoacoustic imaging. *Optic Express*. (2007) 15(25):16657. doi:10.1364/OE.15.016657
48. Oh JT, Li ML, Zhang HF, Maslov K, Stoica G, Wang LV. Three-dimensional imaging of skin melanoma *in vivo* by dual-wavelength photoacoustic microscopy. *J Biomed Optic*. (2006) 11(3):34032. doi:10.1117/1.2210907
49. Wang SM, Ibey BL, Roth CC, Tsyboulski DA, Beier HT, Glickman RD, et al. All-optical optoacoustic microscopy based on probe beam deflection technique. *Photoacoustics*. (2016) 4(3):91–101. doi:10.1016/j.pacs.2016.02.001
50. Wong TTW, Zhang R, Hai P, Zhang C, Pleitez MA, Aft RL, et al. Fast label-free multilayered histology-like imaging of human breast cancer by photoacoustic microscopy. *Sci Adv*. (2017) 3(5):e1602168. doi:10.1126/sciadv.1602168
51. WangZhang R, Chen J, Wang H, Yan M, Zheng W, Song L. Longitudinal label-free optical-resolution photoacoustic microscopy of tumor angiogenesis *in vivo*. *Quant Imag Med Surg*. (2015) 5(1):23–9. doi:10.3978/j.issn.2223-4292.2014.11.08
52. Li L, Shemetov AA, Baloban M, Hu P, Zhu L, Shcherbakova DM, et al. Small near-infrared photochromic protein for photoacoustic multi-contrast imaging and detection of protein interactions *in vivo*. *Nat Commun*. (2018) 9(1):2734. doi:10.1038/s41467-018-05231-3
53. Nguyen VP, Paulus YM. Photoacoustic ophthalmoscopy: principle, application, and future directions. *J Imag*. (2018) 4(12):149. doi:10.3390/jimaging4120149
54. Nam SY, Ricles LM, Suggs LJ, Emelianov SY. *In vivo* ultrasound and photoacoustic monitoring of mesenchymal stem cells labeled with gold nanotracers. *PloS One*. (2012) 7(5):e37267. doi:10.1371/journal.pone.0037267
55. Huang D, Swanson W, Lin WG, Schuman JS, Stinson CP, Chang EA, et al. Optical coherence tomography. *Science*. (1991) 254(5035):1178–81. doi:10.1126/science.1957169
56. Puliafito CA, Yehoshua Z, Gregori G, Puliafito CA, Rosenfeld PJ. Chapter 3–optical coherence tomography. In: SJ Ryan, SR Sadda, DR Hinton, AP Schachat, SR Sadda, CP Wilkinson, et al. editors. *In retina*. 5th ed. London, United Kingdom: W.B. Saunders (2013). p. 82–110.
57. de Boer JF, Leitgeb R, Wojtkowski M. Twenty-five years of optical coherence tomography: the paradigm shift in sensitivity and speed provided by Fourier domain OCT [Invited]. *Biomed Optic Express*. (2017) 8(7):3248. doi:10.1364/BOE.8.003248
58. Fercher AF, Leitgeb R, Hitzenberger CK, Sattmann H, Wojtkowski M. "Complex spectral interferometry OCT," in medical applications of lasers in dermatology, cardiology, ophthalmology, and dentistry II. *Feb*. (1999) 3564:173–8. doi:10.1117/12.339152
59. Aumann S, Donner S, Fischer J, Müller F. Optical coherence tomography (OCT): principle and technical realization. In: JF Bille., editor *High resolution imaging in microscopy and ophthalmology: new frontiers in biomedical optics*. Cham, Switzerland: Springer International Publishing (2019). p. 59–85.
60. Yaqoob Z, Wu J, Yang C. Spectral domain optical coherence tomography: a better OCT imaging strategy. *Biotechniques*. (2005) 39(6 Suppl. l):S6–13. doi:10.2144/000112090
61. Hahn P, Migacz J, O'Connell R, Maldonado RS, Izatt JA, Toth CA. The use of optical coherence tomography in intraoperative ophthalmic imaging. *Ophthalmic Surg Laser Imag*. (2011) 42 Suppl(4):S85–94. doi:10.3928/15428877-20110627-08
62. Pircher M, Zawadzki RJ. Review of adaptive optics OCT (AO-OCT): principles and applications for retinal imaging [Invited]. *Biomed Optic Express*. (2017) 8(5):2536–62. doi:10.1364/BOE.8.002536
63. Ramos JL, Li Y, Huang D. Clinical and research applications of anterior segment optical coherence tomography–a review. *Clin Exp Ophthalmol*. (2009) 37(1):81–9. doi:10.1111/j.1442-9071.2008.01823.x
64. Leitgeb RA, Werkmeister RM, Blatter C, Schmetterer L. Doppler optical coherence tomography. *Prog Retin Eye Res*. (2014) 41:26–43. doi:10.1016/j.preteyeres.2014.03.004
65. Chen CL, Wang RK. Optical coherence tomography based angiography [Invited]. *Biomed Optic Express*. (2017) 8(2):1056–82. doi:10.1364/BOE.8.001056
66. De Boer JF, Hitzenberger CK, Yasuno Y. Polarization sensitive optical coherence tomography–a review [Invited]. *Biomed Optic Express*. (2017) 8(3):1838–73. doi:10.1364/BOE.8.001838
67. Liang X, Boppart SA, Boppart SA. Biomechanical properties of *in vivo* human skin from dynamic optical coherence elastography. *IEEE Trans Biomed Eng*. (2010) 57(04):953–9. doi:10.1109/TBME.2009.2033464
68. Shu X, Liu W, Duan L, Zhang HF. Visible spectroscopic doppler analysis for visible-light optical coherence tomography. *J Biomed Optic*. (2017) 22(12):1. doi:10.1117/1.JBO.22.12.121702
69. Zhang PJ, Bouwens A, Szlag D, Lasser T, Extermann J. Brain imaging with extended-focus optical coherence tomography at different scales and spectral ranges (Conference Presentation). In: Optical coherence tomography and coherence domain optical methods in biomedicine, XXIII; 2019 March 4; San Jose, CA: SPIE BiOS (2019). p. 108671U.
70. Magnain C. Human brain imaging by optical coherence tomography. In: *Handbook of Neurophotonics*., 399. Boca Raton, FL: CRC Press (2020). 448 p.
71. Ling Y, Li C, Purslow C, Yang Y, Huang Z. Evaluation of human corneal ulcer healing process using optical coherence tomography: an *in vitro* study. In: Optical elastography and tissue biomechanics VI; 2019 Feburary 21; San Jose, CA: SPIE BiOS (2019). p. 108801H.
72. Hendon CP, Lye TH, Yao X, Gan Y, Marboe CC. Optical coherence tomography imaging of cardiac substrates. *Quant Imag Med Surg*. (2019) 9(5):882. doi:10.21037/qims.2019.05.09
73. Rajabi-Estarabadi A, Bittar LG, Zheng I, Nascimento V, Camacho C, Feun JM, et al. Optical coherence tomography imaging of melanoma skin cancer. *Laser Med Sci*. (2019) 34(2):411–20. doi:10.1007/s10103-018-2696-1
74. NouriBittar A, Huang D. Optical coherence tomography angiography in neurology and neuro-ophthalmology. In: *OCT and imaging in central nervous system diseases*. AG Switzerland: Springer (2020). p. 523–44.
75. Malone J, Hohert G, Hoang L, Miller DM, McAlpine J, MacAulay C, et al. Endoscopic optical coherence tomography (OCT) and autofluorescence imaging (AFI) of *ex vivo* fallopian tubes. *Multimodal Biomed Imag XV*. (2020) 11232:1123202. 10.1117/12.2544475
76. Freund JE, Buijs M, Bruin DM, Savci-Heijink CD, Rosette JJMCH, Leeuwen TGV, et al. Optical coherence tomography in urologic oncology: a comprehensive review. *SN Comprehen Clin Med*. (2019) 1(2):67–84.
77. Fried D. Optical coherence tomography for imaging dental caries. In *Detection and assessment of dental caries*. Cham, Switzerland: Springer (2019). p. 199–208.
78. Beaurepaire E, Moreaux L, Amblard F, Mertz J. Combined scanning optical coherence and two-photon-excited fluorescence microscopy. *Opt Lett*. (1999) 24(14):969–71. doi:10.1364/OL.24.000969
79. Dunkers J, Cicerone M, Washburn N. Collinear optical coherence and confocal fluorescence microscopies for tissue engineering. *Optic Express*. (2003) 11(23):3074–9. doi:10.1364/OE.11.003074
80. Harper DJ, Augustin M, Lichtenegger A, Eugui P, Glösmann M, Hitzenberger CK, et al. White light optical coherence tomography for sub-micron resolution and spectroscopic imaging in the mouse retina. *Invest Ophthalmol Vis Sci*. (2018) 59(9):5826. 10.1364/BOE.9.002115
81. Marchand PJ, Szlag D, Bouwens A, Lasser T. *In vivo* high-resolution cortical imaging with extended-focus optical coherence microscopy in the visible-NIR wavelength range. *J Biomed Optic*. (2018) 23(3):1–7. doi:10.1117/1.JBO.23.3.036012
82. Wang LV, Hu S. Photoacoustic tomography: *in vivo* imaging from organelles to organs. *Science*. (2012) 335(6075):1458–62. doi:10.1126/science.1216210
83. Wang LV, Yao J. A practical guide to photoacoustic tomography in the life sciences. *Nat Methods*. (2016) 13(8):627–38. doi:10.1038/nmeth.3925
84. Marsh-Armstrong B, Migacz J, Jonnal R, Werner JS. Automated quantification of choriocapillaris anatomical features in ultrahigh-speed optical coherence tomography angiograms. *Biomed Optic Express*. (2019) 10(10):5337–50. doi:10.1364/BOE.10.005337
85. Ma Z, Luo S, Yu M, Liu J, Zhao Y, Yu Y, et al. Assessment of microvasculature flow state with a high speed all-optic dual-modal system of optical coherence tomography and photoacoustic imaging. *Biomed Optic Express*. (2018) 9(12):6103–15. doi:10.1364/BOE.9.006103
86. WangLuo EZ, Povazay B, Laufer J, Alex A, Hofer B, Pedley B, et al. Multimodal photoacoustic and optical coherence tomography scanner using an all optical

detection scheme for 3D morphological skin imaging. *Biomed Optic Express*. (2011) 2(8):2202–15. doi:10.1364/BOE.2.002202
87. DrexlerPovazay BJ, Lanning RM, Tyrrell JA, Padera TP, Bartlett LA, Stylianopoulos T, et al. Three-dimensional microscopy of the tumor microenvironment *in vivo* using optical frequency domain imaging. *Nat Med*. (2009) 15(10):1219–23. doi:10.1038/nm.1971
88. BoumaLanning HS, Yoo H. Spectroscopic optical coherence tomography: a review of concepts and biomedical applications. *Appl Spectrosc Rev*. (2018) 53(2–4):91–111. doi:10.1080/05704928.2017.1324876
89. Morgner U, Drexler W, Kärtner FX, Pitris XD, Ippen C, Fujimoto EP. Spectroscopic optical coherence tomography. *Opt Lett*. (2000) 25(2):111–3. doi:10.1364/OL.25.000111
90. FujimotoDrexler W, Wei Q, Liu W, Liu T, Yi J, Sheibani N, et al. A combined method to quantify the retinal metabolic rate of oxygen using photoacoustic ophthalmoscopy and optical coherence tomography. *Sci Rep*. (2015) 4(1):6525. doi:10.1038/srep06525
91. Zhang ND, Linsenmeier RA. Retinal oxygen: fundamental and clinical aspects. *Arch Ophthalmol*. (2003) 121(4):547–57. doi:10.1001/archopht.121.4.547
92. Hammes H-P. Pericytes and the pathogenesis of diabetic retinopathy. *Horm Metab Res*. (2005) 37 Suppl 1(1):39–43. doi:10.1055/s-2005-861361
93. Mozaffarieh M, Grieshaber MC, Flammer J. Oxygen and blood flow: players in the pathogenesis of glaucoma. *Mol Vis*. (2008) 14:224–33.
94. Wilson KE, Bachawal SV, Tian L, Willmann JK. Multiparametric spectroscopic photoacoustic imaging of breast cancer development in a transgenic mouse model. *Theranostics*. (2014) 4(11):1062–71. doi:10.7150/thno.9922
95. Nguyen VP, Li Y, Qian W, Liu B, Tian C, Zhang W, et al. Contrast agent enhanced multimodal photoacoustic microscopy and optical coherence tomography for imaging of rabbit choroidal and retinal vessels *in vivo*. *Sci Rep*. (2019) 9(1):5945. doi:10.1038/s41598-019-42324-5
96. Nguyen VP, Li Y, Aaberg M, Zhang W, Wang X, Paulus YM. In Vivo 3D imaging of retinal neovascularization using multimodal photoacoustic microscopy and optical coherence tomography imaging–PubMed (2018). Available at: https://pubmed-ncbi-nlm-nih-gov.proxy.lib.uwaterloo.ca/31681820/ (Accessed June 17, 2020).
97. PaulusLi J, Xia J, Maslov KI, Nasiriavanaki M, Tsytsare V, Demchenko AV, et al. Noninvasive photoacoustic computed tomography of mouse brain metabolism *in vivo*. *Neuroimage*. (2013) 64:257–66. doi:10.1016/j.neuroimage.2012.08.054
98. WangXia M, Xia J, Wan H, Bauer AQ, Culver JP, Wang LV. High-resolution photoacoustic tomography of resting-state functional connectivity in the mouse brain. *Proc Natl Acad Sci USA*. (2014) 111(1):21–6. doi:10.1073/pnas.1311868111
99. Jo J, Yang X. Functional photoacoustic imaging to observe regional brain activation induced by cocaine hydrochloride. *J Biomed Optic*. (2011) 16(9):090506. doi:10.1117/1.3626576
100. Marchand PJ, Bouwens A, Szlag D, Nguyen D, Descloux A, Sison M, et al. Visible spectrum extended-focus optical coherence microscopy for label-free sub-cellular tomography. *Biomed Optic Express*. (2017) 8(7):3343. doi:10.1364/BOE.8.003343
101. LasserBouwens PJ, Szlag D, Bouwens A, Lasser T. *In vivo* high-resolution cortical imaging with extended-focus optical coherence microscopy in the visible-NIR wavelength range. *JBO*. (2018) 23(3):036012. doi:10.1117/1.JBO.23.3.036012
102. Hu S, Maslov K, Tsytsarev V, Wang LV. Functional transcranial brain imaging by optical-resolution photoacoustic microscopy. *J Biomed Optic*. (2009) 14(4):040503. doi:10.1117/1.3194136
103. Zabihian B, Weingast J, Liu M, Zhang E, Beard P, Pehamberger H, et al. *In vivo* dual-modality photoacoustic and optical coherence tomography imaging of human dermatological pathologies. *Biomed Optic Express*. (2015) 6(9):3163. doi:10.1364/BOE.6.003163
104. HermannWeingast D, Lee C, Kim S, Zhou Q, Kim J, Kim C. *In Vivo* near infrared virtual intraoperative surgical photoacoustic optical coherence tomography. *Sci Rep*. (2016) 6(1):35176. doi:10.1038/srep35176
105. Cash KJ, Li C, Xia J, Wang LV, Clark HA. Optical drug monitoring: photoacoustic imaging of nanosensors to monitor therapeutic lithium *in Vivo*. *ACS Nano*. (2015) 9(2):1692–8. doi:10.1021/nn5064858
106. Pomerantz R, Zell D, McKenzie G, Siegel DM. Optical coherence tomography used as a modality to delineate basal cell carcinoma prior to Mohs micrographic surgery. *Case Rep Dermatol*. (2011) 3(3):212–8. doi:10.1159/000333000
107. Dahlstrand U, Sheikh R, Merdasa A, Chakari R, Persson B, Cinthio M, et al. Photoacoustic imaging for three-dimensional visualization and delineation of basal cell carcinoma in patients. *Photoacoustics*. (2020) 18:100187. doi:10.1016/j.pacs.2020.100187
108. MalmsjöSheikh M, Drexler W. Optical coherence tomography angiography and photoacoustic imaging in dermatology. *Photochem Photobiol Sci*. (2019) 18(5):945–62. doi:10.1039/C8PP00471D
109. Yoon TJ, Cho YS. Recent advances in photoacoustic endoscopy. *World J Gastrointest Endosc*. (2013) 5(11):534–9. doi:10.4253/wjge.v5.i11.534
110. Gora MJ, Suter MJ, Tearney GJ, Li X. Endoscopic optical coherence tomography: technologies and clinical applications [Invited]. *Biomed Optic Express*. (2017) 8(5):2405–44. doi:10.1364/BOE.8.002405
111. Zackrisson S, van de Ven SMWY, Gambhir SS. Light in and sound out: emerging translational strategies for photoacoustic imaging. *Canc Res*. (2014) 74(4):979–1004. doi:10.1158/0008-5472.CAN-13-2387
112. Wu M, Fw van der Steen A, Regar E, van Soest G. Emerging technology update intravascular photoacoustic imaging of vulnerable atherosclerotic plaque. *Intervent Cardiol*. (2016) 11(2):120–3. doi:10.15420/icr.2016:13:3
113. Li L, Maslov K, Ku G, Wang LV. Three-dimensional combined photoacoustic and optical coherence microscopy for *in vivo* microcirculation studies. *Optic Express*. (2009) 17(19):16450–5. doi:10.1364/OE.17.016450
114. Cai X, Zhang Y, Li L, Choi S-W, MacEwan SW, Yao MR, et al. Investigation of neovascularization in three-dimensional porous scaffolds *in vivo* by a combination of multiscale photoacoustic microscopy and optical coherence tomography. *Tissue Eng C Methods*. (2013) 19(3):196–204. doi:10.1089/ten.TEC.2012.0326
115. WangZhang S, Xie Z, Zhang HF, Puliafito CA. Simultaneous multimodal imaging with integrated photoacoustic microscopy and optical coherence tomography. *Opt Lett*. (2009) 34(19):2961–3. doi:10.1364/OL.34.002961
116. Liu T, Wei Q, Wang J, Jiao S, Zhang HF. Combined photoacoustic microscopy and optical coherence tomography can measure metabolic rate of oxygen. *Biomed Optic Express*. (2011) 2(5):1359–65. doi:10.1364/BOE.2.001359
117. Tsytsarev V, Rao B, Maslov KI, Li L, Wang LV. Photoacoustic and optical coherence tomography of epilepsy with high temporal and spatial resolution and dual optical contrasts. *J Neurosci Methods*. (2013) 216(2):142–5. doi:10.1016/j.jneumeth.2013.04.001
118. Liu M. A study of spectral domain optical coherence tomography and photoacoustic microscopy for biometric and biomedical applications. [Master's thesis]. Newark (United States): University of Delaware (2011).
119. Zhu X, Huang Z, Li Z, Li W, Liu X, Chen Z, et al. Resolution-matched reflection mode photoacoustic microscopy and optical coherence tomography dual modality system. *Photoacoustics*. (2020) 19:100188. doi:10.1016/j.pacs.2020.100188
120. Qin W, Qi W, Jin T, Guo H, Xi L. *In vivo* oral imaging with integrated portable photoacoustic microscopy and optical coherence tomography. *Appl Phys Lett*. (2017) 111(26):263704. doi:10.1063/1.5006234
121. Qin W, Chen Q, Xi L. A handheld microscope integrating photoacoustic microscopy and optical coherence tomography. *Biomed Optic Express*. (2018) 9(5):2205. doi:10.1364/BOE.9.002205
122. Dadkhah A, Jiao S. Optical coherence tomography-guided dynamic focusing for combined optical and mechanical scanning multimodal photoacoustic microscopy. *J Biomed Optic*. (2019) 24(12):1. doi:10.1117/1.JBO.24.12.121906.2019
123. Liu Y, Xu M, Dai Y, Zhao Q, Zhu L, Guan X, et al. NIR-II dual-modal optical coherence tomography and photoacoustic imaging-guided dose-control cancer chemotherapy. *ACS Appl Polym Mater*. (2020) 2(5):1964–73. doi:10.1021/acsapm.0c00155
124. Dong B, Sun C, Zhang HF. Optical detection of ultrasound in photoacoustic imaging. *IEEE Trans Biomed Eng*. (2017) 64(1):4–15. doi:10.1109/TBME.2016.2605451
125. Lee C, Han S, Kim S, Jeon M, Jeon MY, Kim C, et al. Combined photoacoustic and optical coherence tomography using a single near-infrared

supercontinuum laser source. *Appl Optic*. (2013) 52(9):1824–8. doi:10.1364/AO.52.001824

126. Hermann B, Li N, Schmitner B, Meyer D, Weninger WJ, Drexler W, et al. Hybrid ultrahigh resolution optical coherence/ photoacoustic microscopy. *Photon Plus Ultrasound*. (2015) 9323:93232N. doi:10.1117/12.2079232
127. Li L, Dai C, Li Q, Zhao Q, Jiang X, Chai X, et al. Fast subcellular optical coherence photoacoustic microscopy for pigment cell imaging. *Opt Lett*. (2015) 40(19):4448–51. doi:10.1364/OL.40.004448
128. ZhouDai S, Chen Z, Zhao Y, Yang S, Xing D. Simultaneous imaging of atherosclerotic plaque composition and structure with dual-mode photoacoustic and optical coherence tomography. *Optic Express*. (2017) 25(2):530–9. doi:10.1364/OE.25.000530
129. Shu X, Bondu M, Dong B, Podoleanu A, Leick L, Zhang HF. Single all-fiber-based nanosecond-pulsed supercontinuum source for multispectral photoacoustic microscopy and optical coherence tomography. *Opt Lett*. (2016) 41(12):2743. doi:10.1364/OL.41.002743
130. Haindl R, Preisser S, Andreana M, Rohringer W, Sturtzel C, Distel M, et al. Dual modality reflection mode optical coherence and photoacoustic microscopy using an akinetic sensor. *Opt Lett*. (2017) 42(21):4319–22. doi:10.1364/OL.42.004319
131. LiuPreisser S, Rohringer W, Liu M, Kollmann C, Zotter S, Fischer B, et al. All-optical highly sensitive akinetic sensor for ultrasound detection and photoacoustic imaging. *Biomed Optic Express*. (2016) 7(10):4171–86. doi:10.1364/BOE.7.004171
132. DrexlerRohringer R, Deloria AJ, Sturtzel C, Sattmann H, Rohringer W, Fischer B, et al. Functional optical coherence tomography and photoacoustic microscopy imaging for zebrafish larvae. *Biomed Optic Express*. (2020) 11(4):2137–51. doi:10.1364/BOE.390410
133. Liu LV. Multiscale photoacoustic microscopy and computed tomography. *Nat Photon*. (2009) 3(9):503. doi:10.1038/nphoton.2009.157
134. Chen S, Shu X, Nesper PL, Liu W, Fawzi AA, Zhang HF. Retinal oximetry in humans using visible-light optical coherence tomography [Invited]. *Biomed Optic Express*. (2017) 8(3):1415. doi:10.1364/BOE.8.001415
135. Pi S, Camino A, Wei X, Simonett J, Cepurna W, Huang D, et al. Rodent retinal circulation organization and oxygen metabolism revealed by visible-light optical coherence tomography. *Biomed Optic Express*. (2018) 9(11):5851. doi:10.1364/BOE.9.005851
136. JiaCamino J, Li R, Phillips EH, Goergen CJ, Sturek M, Cheng JX. Bond-selective photoacoustic imaging by converting molecular vibration into acoustic waves. *Photoacoustics*. (2016) 4(1):11–21. doi:10.1016/j.pacs.2016.01.002
137. Lee HD, Shin JG, Hyun H, Yu BA, Eom TJ. Label-free photoacoustic microscopy for *in-vivo* tendon imaging using a fiber-based pulse laser. *Sci Rep*. (2018) 8(1):4805. doi:10.1038/s41598-018-23113-y
138. Upputuri PK, Pramanik M. Photoacoustic imaging in the second near-infrared window: a review–PubMed (2019). Available at: https://pubmed-ncbi-nlm-nih-gov.proxy.lib.uwaterloo.ca/30968648/ (Accessed Jun. 18, 2020).
139. Bondu M, Marques MJ, Moselund PM, Lall G, Bradu A, Podoleanu A. Multispectral photoacoustic microscopy and optical coherence tomography using a single supercontinuum source. *Photoacoustics*. (2018) 9:21–30. doi:10.1016/j.pacs.2017.11.002
140. Jiao S, Jiang M, Hu J, Fawzi A, Zhou Q, Shung KK, et al. Photoacoustic ophthalmoscopy for *in vivo* retinal imaging. *Optic Express*. (2010) 18(4):3967–72. doi:10.1364/OE.18.003967
141. ZhangJiang W, Wei Q, Liu T, Kuai D, Burke JM, Jiao S, et al. Integrating photoacoustic ophthalmoscopy with scanning laser ophthalmoscopy, optical coherence tomography, and fluorescein angiography for a multimodal retinal imaging platform. *J Biomed Optic*. (2012) 17(6):061206. doi:10.1117/1.JBO.17.6.061206
142. ZhangWei X, Liu T, Wen R, Li Y, Puliafito CA, Zhang HF, et al. Optical coherence photoacoustic microscopy for *in vivo* multimodal retinal imaging. *Opt Lett*. (2015) 40(7):1370. doi:10.1364/OL.40.001370
143. JiaoLiu DA. The mechanics of human saccadic eye movement. *J Physiol*. (1964) 174(2):245–64. doi:10.1113/jphysiol.1964.sp007485
144. Tian C, Zhang W, Mordovanakis A, Wang X, Paulus YM. Noninvasive chorioretinal imaging in living rabbits using integrated photoacoustic microscopy and optical coherence tomography. *Optic Express*. (15942017) 25(14):15947. doi:10.1364/OE.25.015947
145. Zhang W, Li Y, Nguyen VP, Huang Z, Liu Z, Wang X, et al. High-resolution, *in vivo* multimodal photoacoustic microscopy, optical coherence tomography, and fluorescence microscopy imaging of rabbit retinal neovascularization. *Light Sci Appl*. (2018) 7(1):103. doi:10.1038/s41377-018-0093-y
146. PaulusLi W, Li Y, Yu Y, Derouin K, Qin VP, Nguyen X, et al. Simultaneous photoacoustic microscopy, spectral-domain optical coherence tomography, and fluorescein microscopy multi-modality retinal imaging. *Photoacoustics*. (2020) 20:100194. doi:10.1016/j.pacs.2020.100194
147. PaulusLi VP, Li Y, Zhang W, Wang X, Paulus YM. Multi-wavelength, en-face photoacoustic microscopy and optical coherence tomography imaging for early and selective detection of laser induced retinal vein occlusion. *Biomed Optic Express*. (2018) 9(12):5915. doi:10.1364/BOE.9.005915
148. Nguyen VP, Li Y, Zhang W, Wang X, Paulus YM. High-resolution multimodal photoacoustic microscopy and optical coherence tomography image-guided laser induced branch retinal vein occlusion in living rabbits. *Sci Rep*. (2019) 9(1):10560. doi:10.1038/s41598-019-47062-2
149. Liu M, Maurer B, Hermann A, Zabihian MG, Sandrian B, Unterhuber B, et al. Dual modality optical coherence and whole-body photoacoustic tomography imaging of chick embryos in multiple development stages. *Biomed Optic Express*. (2014) 5(9):3150. doi:10.1364/BOE.5.003150
150. DrexlerMaurer RA, Baumann B. Multimodal optical medical imaging concepts based on optical coherence tomography. *Front Physiol*. (2018) 6:114. doi:10.3389/fphy.2018.00114
151. Zhang EZ, Maurer B, Hermann J, Zabihian A, Sandrian B, Unterhuber B, et al. Multimodal photoacoustic and optical coherence tomography scanner using an all optical detection scheme for 3D morphological skin imaging. *Biomed Optic Express*. (2011) 2(8):2202–15. doi:10.1364/BOE.2.002202
152. DrexlerPovazay J, Wang LV. Small-animal whole-body photoacoustic tomography: a review. *IEEE Trans Biomed Eng*. (2014) 61(5):1380–9. doi:10.1109/TBME.2013.2283507
153. Liu M, Chen Z, Zabihian B, Sinz C, Zhang E, Beard PC, et al. Combined multi-modal photoacoustic tomography, optical coherence tomography (OCT) and OCT angiography system with an articulated probe for *in vivo* human skin structure and vasculature imaging. *Biomed Optic Express*. (2016) 7(9):3390. doi:10.1364/BOE.7.003390
154. Zabihian B, Chen Z, Rank E, Sinz C, Bonesi M, Sattmann H, et al. Comprehensive vascular imaging using optical coherence tomography-based angiography and photoacoustic tomography. *J Biomed Optic*. (2016) 21(9):96011. doi:10.1117/1.JBO.21.9.096011
155. LiuChen W, Chen Z, Yang S, Xing D. Optical biopsy approach to basal cell carcinoma and melanoma based on all-optically integrated photoacoustic and optical coherence tomography. *Opt Lett*. (2017) 42(11):2145. doi:10.1364/OL.42.002145
156. Kratkiewicz K, Manwar R, Rajabi-Estarabadi A, Fakhoury J, Meiliute J, Daveluy S, et al. Photoacoustic/ultrasound/optical coherence tomography evaluation of melanoma lesion and healthy skin in a swine model. *Sensors*. (2019) 19(12):2815. doi:10.3390/s19122815
157. Chen Z, Rank E, Meiburger KM, Sinz C. Non-invasive multimodal optical coherence and photoacoustic tomography for human skin imaging (2017). Scientific Reports. Available from: https://www-nature-com.proxy.lib.uwaterloo.ca/articles/s41598-017-18331-9 (Accessed October 03, 2020).
158. Yang Y, Li X, Wang T, Kumavor PD, Aguirre A, Shung KK, et al. Integrated optical coherence tomography, ultrasound and photoacoustic imaging for ovarian tissue characterization. *Biomed Optic Express*. (2011) 2(9):2551–61. doi:10.1364/BOE.2.002551
159. ZhuLi L, Duan C, Xie H, Jiang H. Miniature probe combining optical-resolution photoacoustic microscopy and optical coherence tomography for *in vivo* microcirculation study. *Appl Optic*. (2013) 52(9):1928–31. doi:10.1364/AO.52.001928
160. Dai X, Xi L, Duan C, Yang H, Xie H, Jiang H. Miniature probe integrating optical-resolution photoacoustic microscopy, optical coherence tomography, and ultrasound imaging: proof-of-concept. *Opt Lett*. (2015) 40(12):2921. doi:10.1364/OL.40.002921

161. Mathews SJ, Little C, Loderc CD, Rakhitc RD, Xia W, Zhang EZ, et al. All-optical dual photoacoustic and optical coherence tomography intravascular probe. *Photoacoustics*. (2018) 11:65–70. doi:10.1016/j.pacs.2018.07.002
162. DesjardinsLittle L, Chen LK, Hosseinaee Z, Bizheva K. "*In-vivo*, non-contact, cellular resolution imaging of the human cornea with line-field SD-OCT at 2.5 kHz frame rate (conference presentation)," in optical coherence tomography and coherence domain optical methods in biomedicine XXIV. *Mar*. (2020) 11228:112280J. doi:10.1117/12.2547884
163. Kawana K, Yasuno Y, Yatagai T, Oshika T. High-speed, swept-source optical coherence tomography: a 3-dimensional view of anterior chamber angle recession. *Acta Ophthalmol Scand*. (2007) 85(6):684–5. doi:10.1111/j.1600-0420.2006.00836.x
164. Auksorius E, Borycki D, Stremplewski P, Liżewski K, Niedźwiedziuk P, Tomczewski BL, et al. *In vivo* imaging of the human cornea with high-speed and high-resolution Fourier-domain full-field optical coherence tomography. *Biomed Optic Express*. (2020) 11(5):2849–65. doi:10.1364/BOE.393801
165. WojtkowskiBorycki W, Liu M, Kumar A, Kamali T, Unterhuber A, Leitgeb RA. Optical coherence tomography today: speed, contrast, and multimodality. *J Biomed Optic*. (2014) 19(7):071412. doi:10.1117/1.JBO.19.7.071412
166. Held G, Preisser S, Akarçay HG, Peeters S, Frenz M, Jaeger M. Effect of irradiation distance on image contrast in epi-optoacoustic imaging of human volunteers. *Biomed Optic Express*. (2014) 5(11):3765–80. doi:10.1364/BOE.5.003765
167. Haisch C, Eilert-Zell K, Vogel MM, Menzenbach P, Niessner R. Combined optoacoustic/ultrasound system for tomographic absorption measurements: possibilities and limitations. *Anal Bioanal Chem*. (2010) 397(4):1503–10. doi:10.1007/s00216-010-3685-9
168. Sangha GS, Hale NJ, Goergen CJ. Adjustable photoacoustic tomography probe improves light delivery and image quality. *Photoacoustics*. (2018) 12:6–13. doi:10.1016/j.pacs.2018.08.002
169. Sowers T, Yoon H, Emelianov S. Investigation of light delivery geometries for photoacoustic applications using Monte Carlo simulations with multiple wavelengths, tissue types, and species characteristics (2020). Available at: https://www-spiedigitallibrary-org.proxy.lib.uwaterloo.ca/journals/journal-of-biomedical-optics/volume-25/issue-01/016005/Investigation-of-light-delivery-geometries-for-photoacoustic-applications-using-Monte/10.1117/1.JBO.25.1.016005.full?SSO=1 (Accessed November 23, 2020).
170. Daoudi K, Berg PJ, Rabot O, Kohl A, Tisserand S, Brands P, et al. Handheld probe integrating laser diode and ultrasound transducer array for ultrasound/photoacoustic dual modality imaging. *Optic Express*. (2014) 22(21):26365–74. doi:10.1364/OE.22.026365
171. Steenbergenvan den Berg L, Yang M, Jiang Y, Li C. Optical fluence compensation for handheld photoacoustic probe: an *in vivo* human study case. *J Innov Opt Health Sci*. (2017) 10(04):1740002. doi:10.1142/S1793545817400028
172. Zhou Y, Liang J, Wang LV. Cuffing-based photoacoustic flowmetry in humans in the optical diffusive regime. *J Biophot*. (2016) 9(3):208–12. doi:10.1002/jbio.201500181
173. Zhang X, Wu X, Adelegan OJ, Yamaner FY, Oralkan Ö. Backward-mode photoacoustic imaging using illumination through a CMUT with improved transparency. *IEEE Trans Ultrason Ferroelectrics Freq Contr*. (2018) 65(1):85–94. doi:10.1109/TUFFC.2017.2774283
174. Laufer J, Zhang E, Raivich G, Beard P. Three-dimensional noninvasive imaging of the vasculature in the mouse brain using a high resolution photoacoustic scanner. *Appl Optic*. (2009) 48(10):D299–306. doi:10.1364/AO.48.00D299
175. Uliana JH, Sampaio DRT, Fernandes GSP, Brassesco MS, Nogueira-Barbosa MHN, Carneiro AAO, et al. Multiangle long-Axis lateral illumination photoacoustic imaging using linear array transducer. *Sensors*. (2020) 20(14):4052. doi:10.3390/s20144052
176. Jeon S, Song HB, Kim J, Lee BJ, Managuli R, Kim JH, et al. *In vivo* photoacoustic imaging of anterior ocular vasculature: a random sample consensus approach. *Sci Rep*. (2017) 7(1):4318. doi:10.1038/s41598-017-04334-z
177. KimSong S, Rim S, Kim Y, Lee BH. Noncontact photoacoustic imaging based on optical quadrature detection with a multiport interferometer. *Opt Lett*. (2019) 44(10):2590–3. doi:10.1364/OL.44.002590
178. Wang Y, Li C, Wang RK. Noncontact photoacoustic imaging achieved by using a low-coherence interferometer as the acoustic detector. *Opt Lett*. (2011) 36(20):3975–7. doi:10.1364/OL.36.003975
179. Wang Y, Hu Y, Peng B, Zhou H, Zhao Y, Ma Z. Complete-noncontact photoacoustic microscopy by detection of initial pressures using a 3×3 coupler-based fiber-optic interferometer. *Biomed Optic Express*. (2020) 11(1):505–16. doi:10.1364/BOE.381129
180. Hosseinaee Z, Le M, Bell K, reza PH. Towards non-contact photoacoustic imaging [Review]. *Photoacoustics*., 20 (2020) 100207. doi:10.1016/j.pacs.2020.100207
181. Dong B, Sun C, Zhang HF. Optical detection of ultrasound in photoacoustic imaging. *IEEE Trans Biomed Eng*. (2017) 64(1):4–15.doi:10.1109/TBME.2016.2605451
182. Eom J, Shin JG, Park S, Rim S, Lee BH. An all-fiber-optic combined system of noncontact photoacoustic tomography and optical coherence tomography. *Sensors*. (2016) 16(5):734. doi:10.3390/s16050734
183. Berer T, Leiss-Holzinger E, Hochreiner A, Bauer-Marschallinger J, Buchsbaum A. Multimodal noncontact photoacoustic and optical coherence tomography imaging using wavelength-division multiplexing. *J Biomed Optic*. (2015) 20(4):46013. doi:10.1117/1.JBO.20.4.046013
184. Eom J, Shin JG, Park S, Rim S, Lee BH. An all-fiber-optic combined system of noncontact photoacoustic tomography and optical coherence tomography. *Sensors*. (2016) 16(5):734. doi:10.3390/s16050734
185. Berer T, Leiss-Holzinger E, Hochreiner A, Bauer-Marschallinger J, Buchsbaum A. Multimodal noncontact photoacoustic and optical coherence tomography imaging using wavelength-division multiplexing. *J Biomed Optic*. (2015) 20(4):46013. doi:10.1117/1.JBO.20.4.046013
186. Hajireza P, Shi W, Bell K, Paproski RJ, Zemp RJ. Non-interferometric photoacoustic remote sensing microscopy. *Light Sci Appl*. (2017) 6(6):e16278. doi:10.1038/lsa.2016.278
187. Abbasi S, Bell K, Haji Reza P. Rapid high-resolution mosaic acquisition for photoacoustic remote sensing. *Sensors*. (2020) 20(4):1027. doi:10.3390/s20041027
188. Reza PH, Bell K, Shi W, Shapiro J, Zemp RJ. Deep non-contact photoacoustic initial pressure imaging. *Optica*. (2018) 5(7):814–20. doi:1364/OPTICA.5.000814
189. Abbasi S, Le K, Sonier G, Dinakaran D, Bigras B, Bell M, et al. All-optical reflection-mode microscopic histology of unstained human tissues. *Sci Rep*. (2019) 9(1):13392–11. doi:10.1038/s41598-019-49849-9
190. Hosseinaee Z, Khalili L, Simmons JAT, Bell K, Reza PH. Label-free, non-contact, in-vivo ophthalmic imaging using photoacoustic remote sensing microscopy. *Opt Lett* (2020) 45:6254–57.
191. Martell MT, Haven NJM, Zemp RJ. Multimodal imaging with spectral-domain optical coherence tomography and photoacoustic remote sensing microscopy. *Opt Lett*. (2020) 45(17):4859–62. doi:10.1364/OL.398940

Conflict of Interest: Author PHR has financial interests in illumiSonics Inc. IllumiSonics partially supported this work.

The remaining authors declare that the research was conducted in the absence of any commercial or financial relationships that could be construed as a potential conflict of interest.